AD_____

Award Number: DAMD17-02-1-0326

TITLE: Electrical Impedance Tomography of Breast Cancer

PRINCIPAL INVESTIGATOR: L. Tugan Muftuler, Ph.D.

CONTRACTING ORGANIZATION: University of California Irvine
                           Irvine, CA 92697-1875

REPORT DATE: June 2005

TYPE OF REPORT: Final

PREPARED FOR: U.S. Army Medical Research and Materiel Command
               Fort Detrick, Maryland 21702-5012

DISTRIBUTION STATEMENT: Approved for Public Release;
                        Distribution Unlimited

20051013 014

	Form Approved
REPORT DOCUMENTATION PAGE	OMB No. 0704-0188

Public reporting burden for this collection of information is estimated to average 1 hour per response, including the time for reviewing instructions, searching existing data sources, gathering and maintaining the data needed, and completing and reviewing this collection of information. Send comments regarding this burden estimate or any other aspect of this collection of information, including suggestions for reducing this burden to Department of Defense, Washington Headquarters Services, Directorate for Information Operations and Reports (0704-0188), 1215 Jefferson Davis Highway, Suite 1204, Arlington, VA 22202-4302. Respondents should be aware that notwithstanding any other provision of law, no person shall be subject to any penalty for failing to comply with a collection of information if it does not display a currently valid OMB control number. **PLEASE DO NOT RETURN YOUR FORM TO THE ABOVE ADDRESS.**

1. REPORT DATE (DD-MM-YYYY) 01-06-2005	2. REPORT TYPE Final	3. DATES COVERED (From - To) 6 May 2002 – 5 May 2005
4. TITLE AND SUBTITLE		5a. CONTRACT NUMBER
Electrical Impedance Tomography of Breast Cancer		5b. GRANT NUMBER DAMD17-02-1-0326
		5c. PROGRAM ELEMENT NUMBER
6. AUTHOR(S)		5d. PROJECT NUMBER
L. Tugan Muftuler, Ph.D.		5e. TASK NUMBER
		5f. WORK UNIT NUMBER
7. PERFORMING ORGANIZATION NAME(S) AND ADDRESS(ES) University of California Irvine Irvine, CA 92697-1875		8. PERFORMING ORGANIZATION REPORT NUMBER
9. SPONSORING / MONITORING AGENCY NAME(S) AND ADDRESS(ES) U.S. Army Medical Research and Materiel Command Fort Detrick, Maryland 21702-5012		10. SPONSOR/MONITOR'S ACRONYM(S)
		11. SPONSOR/MONITOR'S REPORT NUMBER(S)

12. DISTRIBUTION / AVAILABILITY STATEMENT
Approved for Public Release; Distribution Unlimited

13. SUPPLEMENTARY NOTES

14. ABSTRACT

Abstract is on page 4 of the report.

15. SUBJECT TERMS
Diagnosis of Metastatic Cancer, Magnetic Resonance Imaging, Electrical Impedance Imaging, Electrical Impedance Scanning, MRI current Density Imaging, Finite Element

16. SECURITY CLASSIFICATION OF:			17. LIMITATION OF ABSTRACT	18. NUMBER OF PAGES	19a. NAME OF RESPONSIBLE PERSON
a. REPORT U	b. ABSTRACT U	c. THIS PAGE U	UU	32	19b. TELEPHONE NUMBER (include area code)

Standard Form 298 (Rev. 8-98)
Prescribed by ANSI Std. Z39.18

Table of Contents

Abstract

In screening of breast cancer, once abnormalities or lesions are discovered by the X-ray mammogram, generally, other imaging techniques are needed as an adjunct to diagnose the lesion as benign or malignant. It has been shown that cancer cells exhibit altered local electrical impedance. However, existing technology to measure the electrical impedance of the breast relies on a device that has poor spatial resolution. We proposed to map the impedance distribution in the tissue with high spatial resolution, by using it in conjunction with MRI to improve diagnostic accuracy of screening.

During the first phase of this project, we developed necessary MRI pulse sequences, the software to analyze acquired images to extract impedance information and hardware components to inject electrical current synchronized with the MRI scanner. Several different pulse sequences were tested to determine their sensitivity and specificity. A spin-echo based sequence with alternating current injection at ~200Hz was found to be the most efficient among the tested. Various gel phantoms are prepared mimicking the electrical impedance variations in tissues. With these phantoms, spatial resolution and sensitivity of the method to various current amplitudes and impedance perturbations are measured. The method is also tested on a single animal with a malignant tumor. Results demonstrate that the proposed method clearly distinguishes objects separated by 1-2mm providing a good resolution and it can be used with safe current amplitudes (down to 0.5-1mA). Moreover, the method was able to distinguish 50% impedance variations. Therefore, these results support our hypothesis that MRI-impedance imaging can be used to distinguish benign and malignant tissues. In the second phase of the project, we will perform experiments on tumor induced rats.

1. INTRODUCTION:

In screening of breast cancer, once abnormalities or lesions are discovered by the X-ray mammogram, generally, other imaging techniques are needed as an adjunct to diagnose the lesion as benign or malignant. It has been shown that cancer cells exhibit altered local electrical impedance. However, existing technology to measure the electrical impedance of the breast relies on a device that has poor spatial resolution. We proposed to map the impedance distribution in the tissue with high spatial resolution, by using it in conjunction with MRI to improve diagnostic accuracy of screening. For this purpose, we proposed: (1) To develop and optimize the necessary hardware and software for Magnetic Resonance Electrical Impedance Tomography (MREIT) and interface it with the 4T MRI system, (2) Test the method on an animal model of breast cancer and (3) Optimize the imaging parameters for minimizing false negatives and positives.

All the methods proposed in the original application were successfully developed and tested during this project period. Successful conductivity (MREIT) images were obtained both from specially constructed phantoms as well as from animals bearing tumors. The phantoms were prepared such that they mimicked human tissue properties both for MRI and impedance imaging.

A one-year no-cost extension was requested by the PI and granted by the agency to compensate for the time lost due to a serious MRI equipment failure that required substantial upgrades in the system. This extension period allowed us to improve image reconstruction techniques and we developed an iterative technique for improved accuracy, which was not included in the original application.

2. BODY

2.1. The Pulse Sequence:

2.1.1. *First year*:

We have developed the pulse sequences required for performing MREIT experiments. Various pulse sequences have been tested and a spin-echo based sequence with multiple 180^0 RF refocusing pulses was chosen based on the following criteria: 1) Sensitivity to low electrical current amplitudes; 2) Spatial resolution; 3) Speed of acquisition.

As explained in the first year report, the other pulse sequence described in the original proposal was found to be much slower because of the fact that two phase encoding gradients needed to be applied in two orthogonal directions. Besides, spatial resolution had to be sacrificed to keep the experimental duration at a reasonable level for the comfort of the animals.

In the chosen pulse sequence, sinusoidal current is injected into an object and the resulting magnetic fields are measured using a modified spin-echo sequence (Figure 1) [1, 2]. The component of current-generated magnetic field parallel to the main static field (z-component) produces a phase shift. By synchronizing successive π pulses to half cycles of the current, this phase shift accumulates and is given in the final image as $\varphi(\mathbf{r}) = 4 \cdot \gamma \cdot N \cdot b(\mathbf{r}) / \omega$, where γ is the gyromagnetic ratio, N the number of cycles of injected current, $b(\mathbf{r})$ the amplitude of z-component current-generated magnetic field at point $\mathbf{r}$, and ω the angular frequency of the injected current. Hence, measurement of this phase shift allows for calculation of the (z-component) magnetic field distribution.

2.1.2. *Second Year*:

The pulse sequence described above was originally developed for single slice imaging. That was preferred because very short duration non-selective (wide band) RF 180 refocusing pulses could be used. Short duration is required because those pulses are applied at zero crossings of the injected current and long duration would interfere with non-zero values of injected current and cause abnormal slice profile, dephasing within slice, etc. For multi-slice imaging, those hard pulses cause significant spurious echos because they flip spins within the whole volume. In the second year, slice selective 3 lobe sinc pulse and non-selective hard pulse with strong crusher gradients and Carr-Purcell Meiboom-Gill (CPMG) echos were tested for multi-

slice MREIT. It was found that hard pulses with alternating phase ($\pm180^0$) and strong crushers resulted in acceptable slice profile and minimum artifacts. The duration of hard pulses was 250μs.

The pulse sequence developments were in accord with the original application and successful multi-slice MREIT results were obtained with the final version.
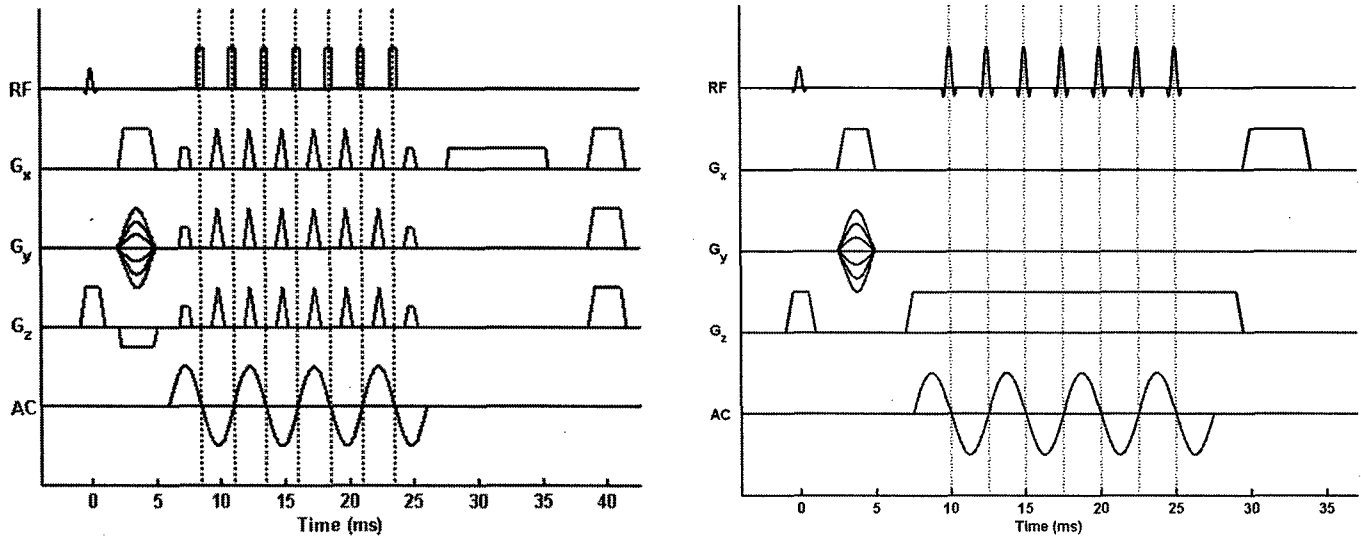

Figure 1 – The two versions of the MREIT pulse sequence for multi-slice conductivity imaging. The one on the left uses hard refocusing RF pulses and the one on the right uses 1.3ms long selective refocusing pulses.

2.2. Reconstruction of Impedance Images and Phantom Experiments:

2.2.1. *First* Year:

A linear approximation $\Delta B(\mathbf{r}) = S(\mathbf{r},\mathbf{r}') \Delta\sigma(\mathbf{r}')$ was assumed, where $\Delta B(\mathbf{r})$ is the change in magnetic field at point $\mathbf{r}$ for a given current injection scheme resulting from a change $\Delta\sigma(\mathbf{r}')$ in the conductivity at point $\mathbf{r}'$. To compute S, the Finite Element Method (FEM) is utilized, whereby the object domain is discretized and S becomes a 'sensitivity' matrix. The matrix component S_{ij} is the change in magnetic field ∂B_i of element i with respect to a change in the conductivity $\partial\sigma_j$ of element j. An initial conductivity distribution σ_0 is assumed (e.g. uniform conductivity), the conductivity of a given element j perturbed by $\Delta\sigma_j$, the resulting ΔB calculated by the FEM, and matrix components approximated as $S_{ij} = \Delta B_i / \Delta\sigma_j$. The linear approximation can be inverted to yield $\Delta\sigma = \sigma_{final} - \sigma_{initial} = S^{-1} \Delta B = S^{-1} (B_{final} - B_{initial})$, where $\sigma_{initial}$ is the assumed initial (uniform) conductivity distribution, $B_{initial}$ the magnetic field distribution given $\sigma_{initial}$ and solved using the FEM, σ_{final} the actual conductivity distribution, B_{final} the MRI measured magnetic field distribution, and S^{-1} a truncated pseudoinverse calculated using singular value decomposition. Hence, the conductivity distribution of an object can be computed as $\sigma_{final} = S^{-1} (B_{final} - B_{initial}) + \sigma_{initial}$.

Experiments:

Several experiments were performed using the spin-echo based sequence and impedance image reconstruction method described above. In these experiments TR was 500ms, TE=30ms and image matrix size was 64x64 with NEX=4. The method was tested on phantoms that were prepared to mimic the tissue conductivities. The goal of these experiments was to identify the spatial resolution and sensitivity of the proposed technique. These phantoms were prepared inside an acrylic cylinder with agarose gels doped with saline solution. A typical phantom was made up of a hollow disk of acrylic with an inner diameter of 7cm and thickness of 1cm, which was filled with a conductive gel of 2% (g/100ml) agarose, 4mM $CuSO_4$, and varying concentrations of NaCl. The plane of the disk was placed perpendicular to the z-axis. 4 electrodes each 5mm wide were placed equidistant along the inner wall of the cylindrical surface and used to inject

currents into the interior region. For each phantom, data was collected for different current injection schemes and used simultaneously in conductivity reconstruction.

MREIT experiments were carried out with different current amplitudes and good quality conductivity images were obtained with amplitudes down to 0.5mA. These initial experiments demonstrated that the method is adequately sensitive to conductivity changes in malignant tissues. In previous studies it was reported that 20-40 fold conductivity changes could be observed in benign versus malignant tissues in humans [3, 4, 5]. Furthermore, these results showed that the method was capable of resolving objects with sizes of a few millimeters.

These results were illustrated in the annual report and also in International Society of Magnetic Resonance in Medicine (ISMRM) conference and included in the appendix for reference.

2.2.2. Second Year:

A series of new phantom studies were conducted to test the spatial resolution and dynamic range of contrast for MREIT. Several agarose gel phantoms with different conductivity distributions were prepared for the tests. The gels were placed inside an acrylic cylinder with an inner diameter of 7cm and height of 1cm. The conductive gels consisted of 2% (g/100mL) agarose and varying concentrations of NaCl. During imaging, the axis of the cylinder was placed parallel to the z-axis (direction of the MRI magnetic field). Four electrodes made of copper foil, each 3mm wide, were placed at 0^0, 90^0, 180^0 and 270^0 along the inner wall and used to inject currents into the interior region. For each phantom, data were collected twice for two current injection schemes and used simultaneously in conductivity reconstruction. The first time, current was injected between the electrodes at 0^0 and 180^0, and the second time between the ones at 90^0, and 270^0. In the preliminary studies conducted, it has been empirically verified that this scheme improves the sensitivity and spatial resolution compared to using a single pair of electrodes.

For contrast studies, a 16mm diameter inner disk of gel surrounded by a background of 1% NaCl was used. Two experiments were carried out with two similar contrast phantoms, where the inner disk contained either 4% or 10% NaCl. In the preliminary tests, it has also been experimentally verified that conductance scales sufficiently linearly with NaCl concentration. Therefore, the conductivity contrast values were approximately 1/4 and 1/10, respectively. A nonlinear relationship was observed between the relative conductivity variations in the actual object versus those calculated by MREIT. The details of these results were given in the second annual report as well as the published article given in the appendix [2]. Fig.2 summarizes these findings.
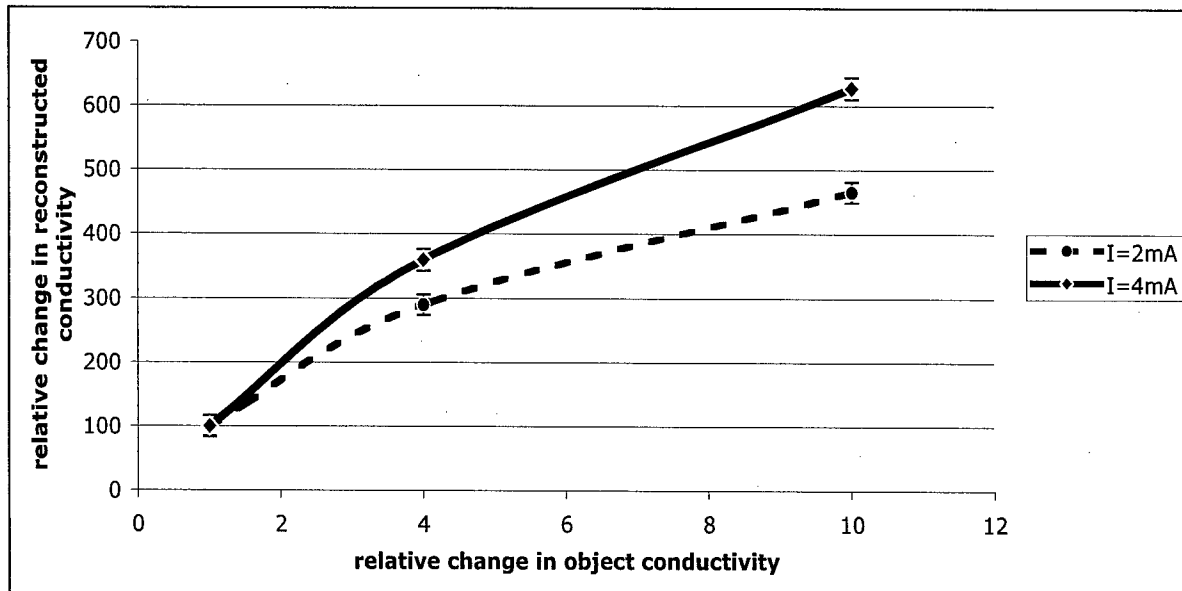

Figure 2. The plots of relative conductivity changes in the object versus relative conductivity values obtained from MREIT images. Plots are given for both of the injected current amplitudes. Error bars are also included in these plots.

2.2.3. *Third Year*:

In the third year, the nonlinear relationship between the relative changes in object conductivity vs reconstructed conductivity was investigated in more detail. Impedance cells were constructed and agarose gels with various NaCl concentrations were measured (Figure 3). Since V_C is a high resistance voltmeter, no current flows through the second electrode pair, thus their contact resistance is negligible. This allowed us to obtain more precise measurement of gel conductivity as a function of NaCl concentration. After each measurement, cells were washed with deionized water and dried to remove all residues before the next measurement. Although our initial measurements revealed almost linear relationship between NaCl concentration and gel conductivity, a more careful examination revealed that some nonlinearity exists. Therefore, our phantom tests were adjusted to account for that small non-linearity. For example, 1g/100ml NaCl concentration yielded 1.2S/m conductivity while 10g/100ml resulted in 10.29S/m, which roughly 8.5 times increase in conductivity instead of 10.
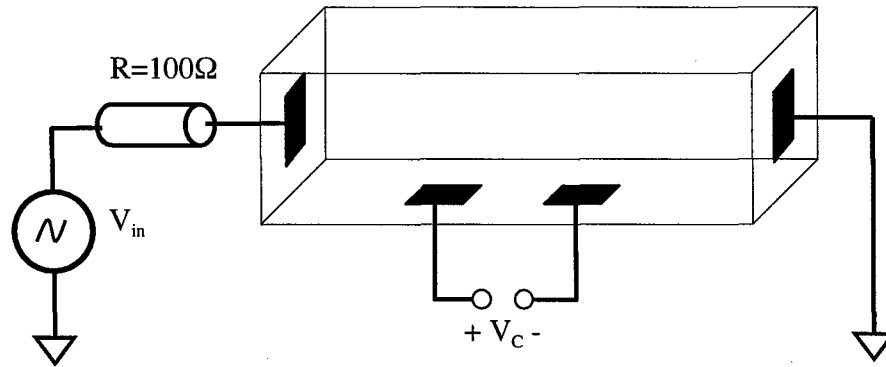

Figure.3. Schematic of the conductivity cell used in measuring the effect of NaCl concentration on agar gel conductivity. Input current is measured over the resistance R and the voltage developed over the second pair of electrodes (V_C) was measured. This eliminates the electrode conductivities in the measurement of gel conductivity.

However, most of the nonlinearity was still accounted for by the linearity assumption in the Sensitivity Matrix based reconstruction. Therefore, we focused our attention to utilize an iterative reconstruction with Tikhonov Regularization. This improved the accuracy as well as spatial specificity of the MREIT images. In summary, the matrix equation was modified with the addition of a *regularization parameter*, λ, and became ($S^T \Delta B = (S^T S + \lambda I) \Delta \sigma$), where I is the identity matrix. This equation was solved for different values of λ using conjugate gradient method and the optimum value of λ was found using L-curve. The conductivity distribution that is calculated after each iteration was assigned as the initial value for the next iteration and the iterations are repeated until the difference between the results of two consecutive iterations are below a predefined threshold. Current was injected from four electrodes placed across the animal's body and six different current distributions were generated by using different combinations of electrode pairs. This scheme also improved the uniformity and sensitivity of the MREIT images. The details of this method and results of phantom experiments were reported in an unpublished abstract prepared by Dr. Birgul and included in the appendix for reference.

These developments are also in accord with the original application. On the other hand, the iterative reconstruction with Tikhonov regularization was not included in the original application but, during the period where the MRI console was malfunctioning we focused our attention to improving the reconstruction technique (see section 2.4).

2.3. In Vivo experiments:

2.3.1. *First Year*:

In the first year, technical developments were completed and a single animal study was conducted for testing. This was in accord with the statement of work proposed in the original application.

The method is tested on a rat with R3230 tumor grown on the left side of its abdomen. First, a standard spin echo image given in Figure 3(b) is acquired. The 2D Finite Element mesh generated with the boundary information extracted from this image (Figure 4(a)) contains 607 nodes and 1096 first order triangular elements. Electrode positions are also found from the spin echo image. For the MR-EIT experiment, 2 cycles of 10mA (rms) 200Hz current were injected into the rat and two phase images were acquired for two current injection cases using TR = 500ms, TE = 30ms, and NEX = 2. In each current injection case one pair of electrodes was used for current injection. After calculating the sensitivity matrix for the generated mesh, inverse problem of MR-EIT was solved. Basis vectors corresponding to singular values less than 1/25 of the maximum singular value were truncated in matrix inversion and the conductivity image in Figure 3(c) was reconstructed.
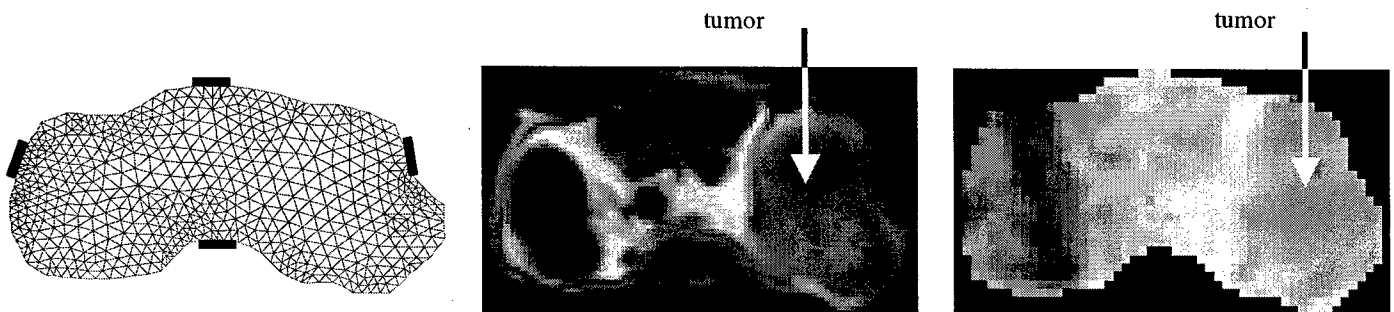

Figure 4 (a) FEM mesh and electrode positions (b) Spin echo image (c) Conductivity image

2.3.2. *Second Year*:

Several MREIT experiments were performed for in vivo impedance imaging of tumor bearing rats. All procedures were approved by the IACUC. For the imaging purpose, a special animal holder was prepared from acrylic sheets. This holder helped keep the animal stationary during imaging. It also allowed for the placement of the electrodes in consistent positions for longitudinal studies. Electrodes were placed on acrylic hollow tubes filled with CuSO4 solution to detect the electrode positions precisely in the images. Initial experience has shown that the precise localization of electrode positions is essential for accurate reconstruction of impedance images. Current carrying wires ran along these tubes, which were in z-direction. This is essential to minimize interference from the magnetic fields generated by current in the wires. Prior to imaging, the animal was anesthetized by IV injection of ketamine and xylazine and then placed inside the holder. The electrodes were covered with a thin layer of conductive gel to provide good electrical contact. The skin areas of contact were shaved for better conductance.

An anatomical image was collected using Fast Spin Echo (FSE) sequence prior to the MREIT images. The data matrix was 256X256, FOV = 10cm, slice thickness = 6mm TR = 4s, TE = 20ms/100ms NEX = 4 (signal averages). MREIT images were collected using the previously outlined pulse sequence with TR=500ms, TE=30ms, NEX=8, 64X64 data matrix, FOV = 10cm, slice thickness = 6mm, with an AC current of 1mA peak, 200Hz, 4 cycles.

Contrast enhanced MR images (CE-MRI) were also collected using MR contrast agent Gd-DTPA. This is a well-established method to detect malignant formations. These images were collected using a gradient-echo sequence with a 64X64 data matrix, FOV = 10cm, 6mm slice thickness, TR = 150ms, TE = 5ms, and 45^0 flip angle. One pre-contrast image was acquired before Gd-DTPA injection and a post-contrast image was collected 3 minutes after injection.

The relative conductivity distribution was computed as described above and overlaid on the anatomical image (Figure 4.a). The resulting images show the higher conductivity regions with high contrast. Similarly,

9

the contrast enhancement by Gd-DTPA is illustrated in figure 4.b. To investigate the spatial correlation of the two images, a third image was generated by masking the CE-MRI image with the MREIT image regions that have conductivity values in the upper one-thirds of the full range. Figure 4.c. shows regions that have high conductivity and also enhanced by Gd-DTPA

Only six animals were imaged in this period and the one shown in Figure 5 yielded the best result. Two of the animal data sets were discarded because of equipment failure during the experiment (see section 2.4). Two data sets were discarded because of large motion artifacts; the other one did not produce good MREIT images. Although the in vivo conductivity images acquired so far were not of diagnostic quality, it demonstrated our capability to carry out such studies. Fig.4 was the first successful in vivo MREIT image of malignancies and demonstrated the potential of MREIT in localizing tumors.

Figure 5. Axial slices from an SD rat inoculated with a R3230 AC tumor showing: (a) Conductivity; (b) CE-MRI; and (c) spatial correlation of CE-MRI and MREIT. The tumor had spread to multiple foci surrounding the body. In (a), red shows high conductivity and blue shows low conductivity regions; whereas red regions in (b) shows enhancement by Gd-DTPA; Areas that have both high conductivity and also enhanced by contrast agent are shown in hot colors in (c).

These initial in vivo experiments revealed several potential problems that were not encountered in phantom tests:

1. Motion artifacts: if the tumor is near the chest area, the motion of the chest during breathing rendered data useless because several pixels overlap when motion is present and phase information is severely compromised.
2. Complex structures like rat abdomen require more than two current injection profiles. In phantoms, cylindrical symmetry and simple structures inside resulted in the least-squares-based reconstruction algorithm to converge to the unique solution. Whereas the reconstruction did not converge to the right solution from the data acquired from a complex animal body. Several simulations were conducted and it was concluded that using different combinations of electrode pairs, six different current injection profiles were created and this allowed us to obtain high quality MREIT images in the third year.

2.3.3. Third Year:

New data were collected from nine rats which were bearing malignant tumors. These tumors were either induced by the carcinogen ENU or R3230 AC tumor grafts. Animals were anesthetized prior to imaging. Structural images were collected using SE sequence prior to MREIT images. The data matrix was 128X128, FOV = 10cm, slice thickness = 4mm, with 2mm gap. TR = 3s, TE = 50ms and NEX = 2 were used. MREIT images were collected using the previously outlined pulse sequence with TR=500ms, TE=30ms, and NEX=12, 64X64 data matrix, FOV = 10cm, slice thickness = 4mm with 2mm gap. 2 cycles of 100Hz current with 1mA rms was applied through different pairs of four electrodes. The resulting images from six animals were illustrated in Figure 6.

For these animals, ROIs (region of interest) were drawn over the tumor region and over the rest of the body. Since these images provide only relative conductivity measures, we took the ratio of mean conductivity in the tumor divided by the mean conductivity elsewhere for each animal. The mean of these

ratios across all animals was μ=2.26, σ=0.62. In other words, the mean conductivity was, on the average, 2.26 times the conductivity in the rest of the body. Some other regions showed relatively high conductivity, which could be out-of-slice effects or could be edema. This will be investigated further.
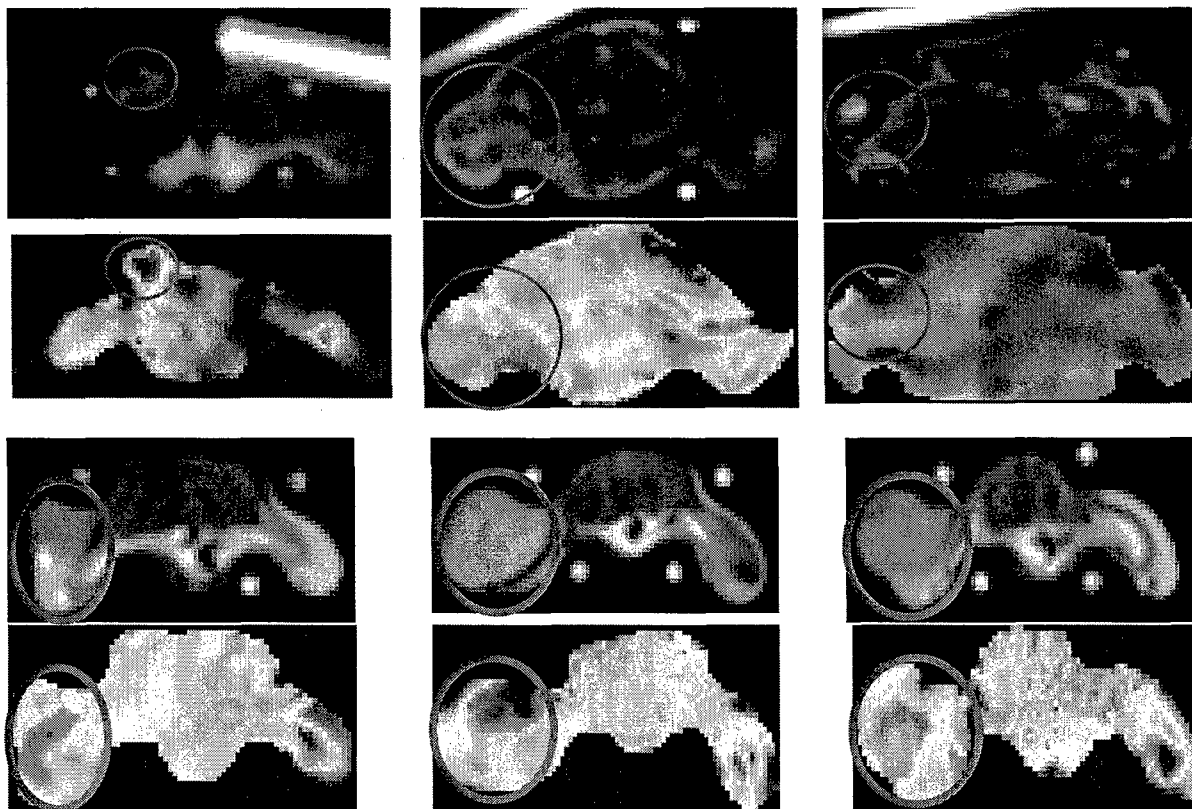

Figure 6. Structural and MREIT images of six animals are illustrated. Anatomic (T2 weighted) scans are displayed in gray levels and corresponding impedance (MREIT) images are depicted in color right below the T2 weighted images. Each image pair shows axial images from different animals. Tumor areas are circled with red lines. Bright objects outside the animals' body were markers to identify exact location of electrodes.

2.4. *Equipment Failures*:

In May-June 2003, we experienced problems in the MRI console RF unit. Several experimental data had to be discarded because of equipment failure at random intervals during data acquisition. We first attempted to repair it ourselves but could not succeed. A repair by the manufacturer was also costly and was not worth for such an old version. Therefore, a new and improved RF unit was ordered and purchased. But all imaging operations had to stop with the Magnetic Resonance Research Systems (MRRS; formerly known as SMIS: Surrey Medical Imaging Systems) console during the period between June and November 2003. The unit was ordered in early August and was shipped at the end of October. By late November, we resumed our experiments but those failures delayed us by at least 6 months. This was explained in the second year report and we are granted a one-year no-cost extension to complete this project successfully.

2.5. Tumor development: Although our group had successfully developed ENU induced tumors before, during this project period only a six of twenty Sprague-Dawley rats developed the tumor. Therefore, we obtained another batch of rats and inoculated them with R3230 AC tumor grafts to proceed with the study. The reasons for failing to develop the targeted amount of malignancies will be discussed with tumor biologists and necessary precautions will be taken to achieve the target tumor development.
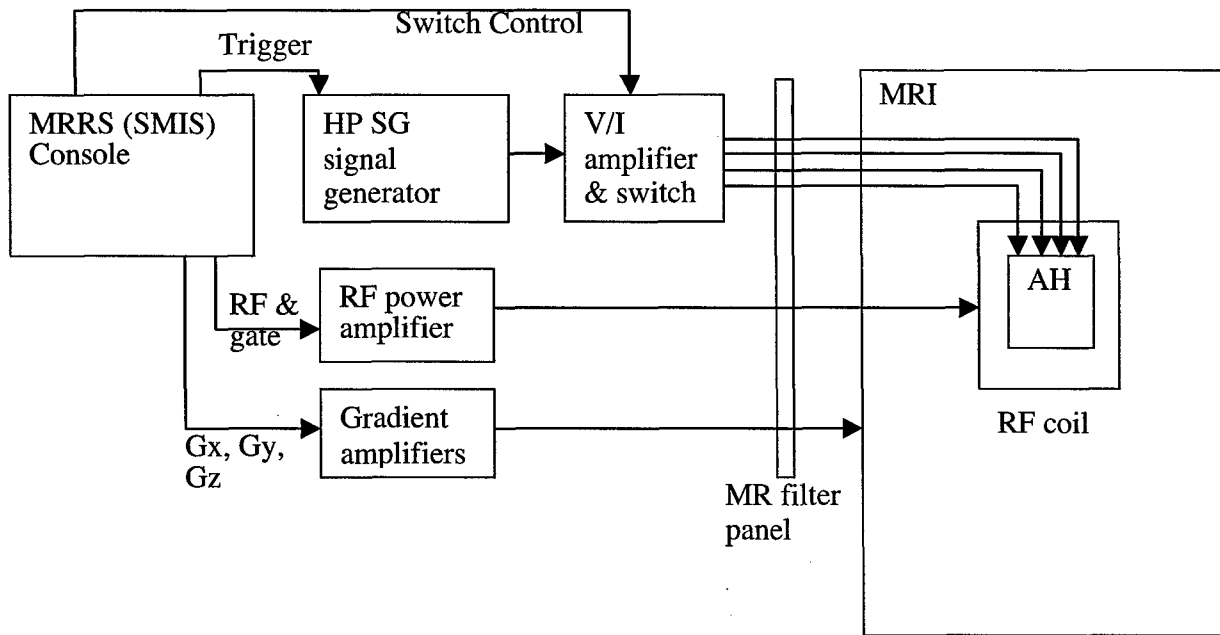
Figure 7. Schematic of the hardware setup. All timing and pulse sequence controls were performed by the SMIS console. Burst sine waves were generated by an HP

2.6. Hardware Setup

The 4T magnet is interfaced with a MRRS Console (Magnetic Resonance Research Systems, Surrey, UK), which controls all gradients and RF pulses, receives the MRI signal, and triggers the signal generator (HP ESG-4400B). Specific pulse sequences are programmed into the console to control these events and their timings.

Figure 7 illustrates the schematic of the hardware setup. The basic operation is described here: When triggered by the MRRS Console, the signal generator outputs a burst sine wave. The user manually enters the frequency, voltage amplitude, and duration of this output. The output of the signal generator is fed into a voltage-to-current converter circuit (transconductance amplifier). This circuit outputs a current whose amplitude is controlled by the input voltage. This current is then delivered to the sample within the MR Scanner. Therefore, output current is independent from the load impedance, as long as the amplifiers do not saturate. Various electrode pairs were selected automatically by a TTL pulse sent from the MRI console to generate six different current patterns in the object. These current lines were filtered by three stages of low pass filters to avoid RF pulses being fed back to MREIT circuitry. Raw data are collected and saved by the MRRS Console, then exported to a separate PC for analysis using developed MATLAB algorithms.

3. KEY RESEARCH ACCOMPLISHMENTS
- Optimum pulse sequence was determined for highest sensitivity, high spatial resolution and short acquisition duration. Multi-slice acquisition was also developed for future 3D FEM based reconstruction that will improve the sensitivity and accuracy of impedance images further.
- Hardware components are designed and implemented for impedance imaging using MRI.
- Sensitivity limit of this pulse sequence to conductivity perturbations was determined with phantom tests.
- Limits of spatial resolution was determined with phantom tests.
- Method is tested on a total of 16 animals and conductivity images were obtained. Some data had to be discarded due to motion or other image artifacts. From the remaining animals, MREIT images show high conductivity in tumors as hypothesized in the original proposal.

12

4. REPORTABLE OUTCOMES:

- Two conference papers were peer-reviewed and accepted for presentation and publication in conference proceedings in the 2003 conference of International Society of Magnetic Resonance in Medicine (ISMRM).
  - o O. Birgul, L. T. Muftuler, M. Hamamura, O. Nalcioglu *"MR-EIT of Malignant Tumors in Rats"*, Proceedings of the International Society for Magnetic Resonance in Medicine 11th Scientific Meeting, pp.1228, Toronto, Canada 2003.
  - o M. Hamamura, L. T. Muftuler, O. Birgul, O. Nalcioglu *"Assessment of the Efficacy of Electrical Impedance Imaging Using MRI"*, Proceedings of the International Society for Magnetic Resonance in Medicine 11th Scientific Meeting, pp.1121, Toronto, Canada 2003.
- One conference paper was peer-reviewed and accepted for presentation and publication in conference proceedings in the 2004 conference of International Society of Magnetic Resonance in Medicine (ISMRM).
  - o L. T. Muftuler, M. Hamamura, O. Birgul, and O. Nalcioglu *"A Comparison of MRI Based Electrical Impedance Imaging and Contrast Enhanced MRI of Tumors"*, Proceedings of the International Society for Magnetic Resonance in Medicine 12th Scientific Meeting, pp.1986, Kyoto, Japan, 2004.
- One manuscript is published in "Technology in Cancer Research and Treatment" Journal.
  - o L. Tugan Muftuler, Mark Hamamura, Ozlem Birgul, Orhan Nalcioglu, *"Resolution And Contrast In Magnetic Resonance Electrical Impedance Tomography (MREIT) and Its Application To Cancer Imaging"*, Technology in Cancer Research and Treatment, v 3 (2), 599-610, (2004).
- Two conference papers were peer-reviewed and accepted for presentation and publication in conference proceedings in the 2005 conference of International Society of Magnetic Resonance in Medicine (ISMRM). The study will also be presented in the 2005 Era of Hope meeting.
  - o Muftuler L T, Hamamura M, Birgul O, and Nalcioglu O, "MRI Based Electrical Impedance Imaging of Tumors with Iterated Sensitivity Reconstruction using Regularization," Proceedings of the International Society for Magnetic Resonance in Medicine 13th Scientific Meeting, pp.2356, Miami, 2005.Hamamura M, Muftuler T, Birgul O, and Nalcioglu O, "Tracking of Sodium Changes Using MR-EIT," Proceedings of the International Society for Magnetic Resonance in Medicine 13th Scientific Meeting, pp.2357, Miami, 2005.
  - o Muftuler L T, Hamamura M, Birgul O, and Nalcioglu O, "MRI Based Electrical Impedance Imaging of Tumors," *to be presented at Era of Hope DOD Breast Cancer Research Program Meeting*, Philadelphia PA, June 8-11, 2005.
- Based on the preliminary data obtained from this grant, the PI has just recently received and NIH R01 grant to investigate this novel idea further.
  - o *"In-Vivo Conductivity Imaging of Tumors with MREIT"* Principal Investigator: L.T. Muftuler Type: NIH R01-CA114210-01 Period: April 2005- March 2009.

Two more manuscripts are in preparation; one is on the results of in vivo studies and the other describes resolution and contrast of MREIT with the iterated reconstruction with regularization. Once ready for submission, copies could be provided to the agency.

5. PROJECT PERSONNEL:

L. Tugan Muftuler (PI)
Orhan Nalcioglu (investigator)
Ozlem Birgul (PGR)
Mark Hamamura (Ph.D. Student)
Mine Demir (project coordinator; originally I. Cruse was named, Ms Demir replaced her)
Huali Wang (animal technician; originally June Wang was named, Ms Wang replaced him)

6. CONCLUSIONS:

During the first phase of this project, we successfully prepared all the required hardware and software components. The limitations and performance of the method was tested and it was verified that the method offers potential to be used for in vivo conductivity imaging of lesions to identify malignancy.

During the second phase of this project, we modified the pulse sequence for multi-slice acquisition for future improvements such as 3D reconstruction. 2D Reconstruction has limitations and it is prone to errors due to contamination from out-of-slice currents. Further investigations were carried out on phantoms to assess limitations and performance (SNR, linearity, etc) of the original reconstruction method. More robust reconstruction with regularization was developed to minimize artifacts.

RF unit failure delayed our studies by about six months and several data were discarded that were acquired during the beginning of these failures. One-year no-cost extension was requested and granted to complete the project.

Although the animal model of breast cancer used in this project is a suitable one to test this novel idea, it also brought the motion artifact problem, which can easily be avoided in actual human studies. In breast imaging, the breasts are stationery and chest motion can be kept outside the images of breasts by selecting phase encoding in the left-right direction. However, in future tests with animal models, we plan to utilize motion correction schemes such as navigator echoes to minimize the errors caused by motion. Moreover, the abdominal region of a rat is a more complicated structure compared to a woman's breast, when all the internal organs and their inherent motion are considered. Therefore, we expect the MREIT images to be more accurate in human breast imaging.

The quality and accuracy of conductivity images can be further improved by utilizing 3D FEM based reconstruction. Some of the residual noise or artifacts in the conductivity images could be due to the contamination (superposition) of magnetic fields generated by currents flowing out of the imaging slice. This can only be modeled by 3D FEM and reconstructed accurately. However, during the limited time of this idea award, 3D FEM models and reconstruction was not attempted. 3D FEM based reconstruction will be developed in our future studies.

The outcomes obtained are in accord with our hypothesis and we have successfully completed the steps outlined in the original project proposal. This was an Idea Award and the main goal of the project has been achieved. We have demonstrated that the proposed MREIT method can be used to identify malignant tumors, which are known to possess high electrical conductivity with respect to healthy tissues. Good quality impedance images were obtained from tumor-bearing rats.

Due several unexpected problems, we could not collect data from the target number of 55 animals. Basically, the failure in obtaining the target number of ENU induced tumors and unexpected equipment failure played a role in missing the target number. Moreover, we ordered the animals in small batches and ran a series of experiments, observed the outcome and delayed the order of next batch if success rate was low. We spent some time to sort out the problems and improve both the hardware and software before we proceeded with the order of the next batch. But, other than missing the target number of animals, all goals have been achieved.

Optimization of pulse sequence parameters and current injection scheme was not done at the end, but rather it went in parallel with technical developments and experiments. As mentioned above, improved reconstruction technique, six current injection profiles, applied current amplitude and frequency were optimized as we proceeded with sets of experiments.

At this stage, we conclude that MREIT cannot be used as a standalone diagnostic tool, but can be used as an adjunct to standard MR scans to improve diagnostic accuracy. To the best of our knowledge, our research group is the only one to demonstrate potential use of MR based impedance imaging in diagnosing or characterizing tumors. The method is still in its early development stages. Further refinements of this technique could improve accuracy more and may reveal important information about the tumor characteristic that cannot be observed with other techniques. As noted in the reportable outcomes, the PI just recently received an NIH R01 grant to investigate this novel idea further.

REFERENCES:

[1] Mikac U. et al, MRI 19: 845 856 (2001).

[2] L. Tugan Muftuler, Mark Hamamura, Ozlem Birgul, Orhan Nalcioglu, *"Resolution And Contrast In Magnetic Resonance Electrical Impedance Tomography (MREIT) and Its Application To Cancer Imaging"*, *Technology in Cancer Research and Treatment,* v 3 (2), 599-610, (2004).

[3] Malich, T. Fritsch, R. Anderson, T. Boehm, M. G. Freesmeyer, M. Fleck, and W. A. Kaiser, "Electrical impedance scanning for classifying suspicious breast lesions: first results," *European Radiology*, vol. 10, pp. 1555-61, 2000.

[4] Malich, T. Boehm, M. Facius, M. G. Freesmeyer, M. Fleck, R. Anderson, and W. A. Kaiser, "Differentiation of mammographically suspicious lesions: evaluation of breast ultrasound, MRI mammography and electrical impedance scanning as adjunctive technologies in breast cancer detection," *Clinical Radiology*, vol. 56, pp. 278-83, 2001.

[5] J. Surowiec, S. S. Stuchly, J. B. Barr, and A. Swarup, "Dielectric properties of breast carcinoma and the surrounding tissues," *IEEE Transactions on Biomedical Engineering*, vol. 35, pp. 257-63, 1988.

Iterated Sensitivity Reconstruction with Tikhonov Regularization for Magnetic Resonance Electrical Impedance Tomography

O. Birgul[1], L. T. Muftuler[1], M. Hamamura[1], O. Nalcioglu[1]

[1]Tu & Yuen Center for Functional Onco Imaging, University of California Irvine, Irvine, CA, United States

Purpose

Electrical conductivity of tissues is significantly different between normal, malignant, and benign tissues. In-vivo impedance imaging of suspicious lesions could aid in diagnosis and specification of malignant tumors. Electrical impedance tomography and electrical impedance spectroscopy are widely used techniques to estimate conductivity values, however, both have low resolution. Measurement of conductivity using magnetic resonance imaging techniques is a recent approach that has the capability of reconstructing high-resolution conductivity images. Magnetic resonance electrical impedance tomography (MREIT) solves the non-linear inverse problem of finding conductivity distribution from MR phase images. In this study, our aim is to develop an improved reconstruction algorithm for MREIT that handles the non-linear nature of the problem using an iterated approach and to quantify the improvement using phantom experiments.

Methods

Low amplitude sinusoidal current is injected into an object and the resulting magnetic field accumulates additional phase in the MR images. A modified fast spin-echo sequence [1], where a 90° RF pulse is followed by a number of 180° (π) RF pulses, is used to measure the magnetic field. Phase induced in positive and negative current cycles would cancel out each other unless multiple π are used. By synchronizing successive π pulses to half cycles of the current, this phase shift accumulates and is given in the final image as $\varphi(\mathbf{r}) = 4 \cdot \gamma \cdot N \cdot b(\mathbf{r}) / \omega$, where γ is the gyromagnetic ratio, N the number of cycles of injected current, $b(\mathbf{r})$ the amplitude of z-component current-generated magnetic field at point $\mathbf{r}$, and ω the angular frequency of the injected current. Therefore, magnetic field distribution is simply the scaled phase MR image.

An iterated sensitivity matrix based algorithm is developed. Images reconstructed using sensitivity approach have been presented in several studies at different field strengths before [2,3]. The localization was good in these images but the reconstructed values were below expected due to linearization approximation in the sensitivity approach. Using appropriate iterations, the true contrast ratios can be calculated. The noise in reconstructed conductivity images effect the divergence of the algorithm, hence, a regularization scheme, such as Tikhonov, must be used. These are taken into consideration in the development of the new algorithm.

Uniform conductivity distribution is assumed and sensitivity matrix is calculated analytically. Resulting matrix equation is given as $S\Delta\sigma=\Delta\mathbf{b}$, where $\Delta\mathbf{b}$ is the difference between measured magnetic field and the magnetic field corresponding to initial distribution, $\Delta\sigma$ is the change with respect to initial and S is the sensitivity matrix, which gives the relation between changes in magnetic field and conductivity. Including Tikhonov regularization parameter λ, the matrix equation becomes $(S^T S+\lambda I)\Delta\sigma=S^T\Delta\mathbf{b}$, where I is the identity matrix. The matrix equation is solved for different values of λ using conjugate gradient method and the optimum regularization value is found using L-curve method. Calculated conductivity distribution is assigned as the initial value and the steps starting with sensitivity matrix calculation are repeated until the change in conductivity two consecutive iterations are below a defined threshold.

Results

Several agarose gel phantoms are prepared with different conductivity values to assess the performance of the developed iterated algorithm. Contrast phantoms, with a 1.6 cm diameter disk surrounded by a background of 1% NaCl was used. The disk contained 10% NaCl (10:1 contrast) and 4% NaCl (4:1 contrast) in two cases. 4 cycles of 4mA (rms) 200Hz current was injected into the phantom using the previously outlined pulse sequence with the parameters TR=500ms, TE=30ms, and NEX=4. The z-component current-generated magnetic field distribution was calculated from the resulting data and the conductivity distribution was computed. The background conductivity is taken as 1mS/cm. Reconstructed peak object values for different iterations are summarized in Table 1. Peak values are 59% and 37% of the true conductivity values for 4:1 and 10:1 contrast values if no iteration is carried out. The algorithm converges at 4th and 6th iterations for 4:1 and 10:1 cases respectively. Images reconstructed at first, second and fifth iterations for 10:1 contrast case are given in Figure 1. Profile images passing through the object are given in Figure 1(d) for five iterations, dashed line being the fifth.

Table 1 Reconstructed peak object values for different contrast levels. Background value is 1mS/cm and object values are 4mS/cm and 10S/cm for 4:1 and 10:1 cases, respectively.

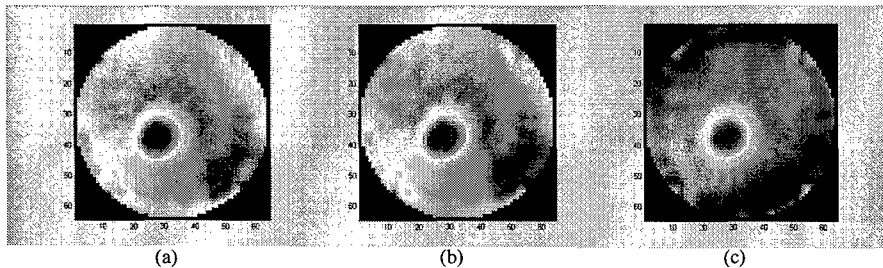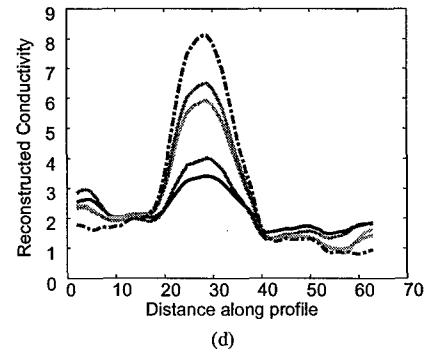| Iter no	4:1	10:1
1	2.36	3.72
2	3.40	4.50
3	3.98	6.27
4	4.00	6.85
5	-	8.49
6	-	8.49

(a)   (b)   (c)

(d)

Figure 1 Reconstructed conductivity images for 10:1 contrast case for different iterations (a) first iteration, (b) second iteration (c) fifth iteration (d) Profile images for first five iterations

Discussion

In this study, an iterative reconstruction algorithm for MREIT was implemented to improve image reconstruction. Malignant tumors have conductivity values 20-40 times larger than the benign and normal tissues and finding the true contrast is important in specification. From Table 1, it is seen that sensitivity approach underestimates the conductivity at first iteration due to its non-linear nature, however, can be improved using iterated approach. Tikhonov regularization gives satisfactory results in solving the ill-conditioned matrix equation. From Figure 1(a)-(c), it is seen that iterations not only provides not only more accurate results but also reduces the background noise in reconstructed conductivity images. These results indicate that iterated sensitivity algorithm could be used in MREIT in cancer applications where high conductivity contrast between background and tumor is present.

References

[1] Malich A, et. al., Eur. Radiol, 10: 1555-1561 (2000), [2] Muftuler L T, et. al.,TCRT December 2004 (in print) [3] Birgul O, et. al. Physics in Med. and Biol, 48: 3485-2504 (2003)

Resolution And Contrast In Magnetic Resonance Electrical Impedance Tomography (MREIT) and its Application To Cancer Imaging

www.tcrt.org

L. Tugan Muftuler, Ph.D.*
Mark Hamamura, M.Sc.
Ozlem Birgul, Ph.D.
Orhan Nalcioglu, Ph.D.

Tu & Yuen Center for
Functional Onco-imaging
164 Irvine Hall
University of California
Irvine CA 92697

It has been reported that the electrical impedance of malignancies could be 20-40 times lower than healthy tissues and benign formations. Therefore, *in vivo* impedance imaging of suspicious lesions may prove to be helpful in improving the sensitivity and specificity of detecting malignant tumors. Several systems have been developed to map the conductivity distribution inside a volume of tissue, however they suffer from poor spatial resolution because the measurements are taken only from surface electrodes. MRI based impedance imaging (MREIT) is a novel method, in which weak electrical currents are injected into the tissue and the resulting perturbations in the magnetic field are measured using MRI. This method has been shown to provide better resolution compared to previous techniques of impedance imaging because the measurements are taken from inside the object on a uniform grid. Thus, it has the potential to be a useful modality that may detect malignancies earlier. Several phantom imaging experiments were performed to investigate the spatial resolution and dynamic range of contrast of this technique. The method was also applied to a live rat bearing a R3230 AC tumor. Tumor location was identified by contrast enhanced imaging.

Key words: Electrical Impedance Tomography, MRI, Cancer imaging.

Introduction

Breast cancer is the leading cause of cancer deaths among women in many parts of the world and currently no single imaging modality has both high sensitivity and specificity for the diagnosis of breast cancer. At present, well-established breast screening methods have high sensitivity but suffer from poor specificity. X-ray mammography, which is accepted as the gold standard for breast cancer screening, provides high sensitivity but has a high rate of false-positives (2-4). Similarly, the sensitivity of breast MRI can be very high, however the specificity for the detection of abnormalities is variable (5, 6). In addition to the high rate of false positives, some of these techniques also fail to detect breast cancer in some cases, such as patients with dense breast tissue, which is common among younger patients, and patients undergoing hormone replacement therapy during post-menopausal period (7). New imaging modalities with better specificity may help reduce the rate of false positives, hence eliminate unnecessary biopsies.

* Corresponding Author:
L. Tugan Muftuler
Email: muftuler@uci.edu

Abbreviations: MRI, Magnetic Resonance Imaging; EIT, Electrical Impedance Tomography; MREIT, Magnetic Resonance Electrical Impedance Tomography; FEM, Finite Element Method; EIS, Electrical Impedance Scanning; OPAMP, Operational Amplifier; SVD, Singular Value Decomposition; NEX, Number of Excitations; CE-MRI, Contrast Enhanced MRI.

It has been shown that electrical properties of malignant tissues are significantly different from those of normal and benign tissues. Surowiec et al. (1) have reported that the electrical impedance of malignant tumors decreases by a factor of 20 to 40 with respect to normal or benign tissues. This information may be used in tumor detection and characterization. Therefore, the spatial distribution of conductivity measurements (which is inversely related to impedance) can be used in conjunction with other imaging modalities to identify tumors and achieve higher specificity rates compared to the currently used techniques.

Electrical Impedance Scanning (EIS) is a new technique recently introduced to aid in the diagnosis of malignant breast tumors (12-15, 26). The device that uses this technique generates a map of the conductivity distribution inside the breast tissue. This device received FDA approval recently and has been introduced to the market (15). A probe that comprises of an array of electrodes is placed over the breast and small amounts of current are injected into the tissue through another electrode placed in the palm of the patient. The magnitude and phase of the current is measured at one electrode at a time and all electrodes are scanned sequentially. Using the distribution of electric currents in this electrode array, a conductivity map is reconstructed; but it does not provide tomographic images. Therefore, the conductivity maps reconstructed using this technique have poor spatial resolution and the spatial resolution is not uniform throughout the imaging region. The generated maps of conductivity are insensitive to tumors deep inside the breast, which are located 3-3.5cm away from the surface. Moreover, tumors just under the nipple are confounded by the high conductivity of the nipple.

Electrical Impedance Tomography (EIT) was developed in the 1980s to reconstruct the conductivity distribution inside a conducting volume. In this method, a current distribution is generated inside the object by injection or induction and peripheral voltage measurements are acquired using limited number of surface electrodes to find the internal conductivity distribution (8). This method also suffers from poor spatial resolution due to the limited number of voltage measurements taken only from the surface. This imaging technique is also less sensitive to conductivity changes deep inside the object. Cherepenin et al. (9) have recently investigated the potential of this technique in breast cancer detection. They have developed an improved EIT system with 256 electrodes placed on a planar surface for improved spatial resolution. They collected in vivo, multi-slice tomographic impedance images of healthy and cancerous breasts. Two remote electrodes were placed on patient's extremities for current injection and voltage reference. This allowed using the assumption of spherical equipotential surfaces near the electrode array. Filtered backprojection along these equipotential surfaces were used for fast 3D image reconstruction. This

device measured only the magnitude of voltage measurements, so the phase information was ignored. This setup helped improve image quality and they were able to detect high conductivity tumor formations of 3-5 cm in size. However, the system still lacks high resolution to detect tumors less than a few centimeters. Moreover, the electrodes with bad contacts cause significant image artifacts. They developed a thresholding technique to detect such electrodes and discard information from them.

Estrela et al. (10), and Kerner et al. (11) have studied electrical properties of breast tumors using an EIT system in which both the magnitude and phase of input current and surface voltage measurements were recorded. Sinusoidal input currents were applied where the frequency was changed between 10KHz up to about 1MHz in discrete steps. This allowed imaging both conductivity and permittivity of breast tissues. Typically, 16 surface electrodes were used that were placed on a circular ring, which resulted in lower spatial resolution compared to (9). However, it was noted that permittivity information was more useful compared to their conductivity counterparts in detecting malignancies.

MREIT is a recently developed method for conductivity imaging (16-21). It uses the magnetic flux density measurements acquired from MR phase images to reconstruct conductivity. Magnetic flux density generated by applied currents can be measured with high spatial resolution using MRI. Various techniques have been proposed for DC (22), AC (23, 24), and RF (25) currents. Unlike EIT, the spatial resolution in the MREIT is position independent. However, it should be noted that only the component of the magnetic flux density in the direction of the main field of the MRI system can be measured. Therefore, one must develop a technique to solve the inverse problem of finding the conductivity or current density from only one component of magnetic flux density. With this technique, only the relative conductivity values can be reconstructed from using only the magnetic flux density measurements. In order to find the absolute conductivity values, at least one voltage measurement from the boundary is required. The reconstruction algorithms can also be divided into two groups depending on the data type required. The first group uses magnetic flux density directly, whereas in the second one, the current density distribution is required in image reconstruction. Algorithms that use current density distribution requires the measurement of all three components of the magnetic flux density, thus rotation of the object inside the magnet is required. All three orthogonal components of the magnetic field have to be measured in order to calculate the current density or precise conductivity distribution. However, this is not a practical situation, especially for human subjects. Rotation would also introduce problems with registration of measurements taken at different orientations of any object under investigation.

Thus, a method that uses only the z-component of the magnetic field to calculate the conductivity distribution (16, 20) was adopted in this study. This method assumes a linear relationship between the measured magnetic fields and relative conductivity perturbations.

In the presented study, the MREIT technique was tested on various conductivity phantoms to investigate its spatial resolution, signal-to-noise ratio (SNR) and contrast-to-noise ratio (CNR). Various phantoms were built with agarose gels mixed with NaCl to create compartments with known conductivity distributions. Preliminary data was also collected *in vivo* from Sprague-Dawley rats innoculated with the R3230 AC tumor. Contrast Enhanced MRI images were also collected to localize the tumor and investigate the spatial correlation between the outcomes of the two techniques.

Materials and Methods

Data were collected by a 4T whole body MRI system that has a Magnex magnet (Magnex Scientific Inc., UK) equipped with a whole body gradient coil set (Tesla Eng. UK), which provides up to 3G/cm gradient fields. The clear bore size of the magnet with gradient assembly is 650mm. A 13 channel room-temperature high-order shim system with MXA-13-4 shim power supply (Resonance Research, Billerica, MA) is also available to minimize field inhomogeneities. This system is interfaced with a MRRS console (Magnetic Resonance Research Systems, Guildford, UK) that has broadband RF transmit and receive channels. A 16 leg, quadrature, high-pass birdcage coil with 10 cm diameter and 18 cm length was designed and built in-house for the MREIT experiments.

Pulse Sequence

The pulse sequence used for the MREIT experiments is similar to a fast spin echo sequence, where a train of 180° RF pulses is applied following a 90° RF pulse (Fig. 1). However, no phase encode or read-out gradients were applied between the 180° RF pulses and the data was collected with a single read-out gradient only after the last 180° RF pulse. Burst sine wave currents were injected into the object during the RF pulse train where each 180° RF pulse was applied at the zero crossing of the sine waves. The duration of each 180° RF pulse was 1.3ms. A similar sequence was proposed by Mikac *et al.* to obtain image of electric currents inside an object (24).

The z-component of magnetic field (parallel to the main static field) generated by the injected currents introduces a phase shift that accumulates over each half-cycle of the sine wave. The simplified MRI signal equation is given as:

$$s(u,v) = \iint M(x,y)\ e^{j\theta(x,y)}\ e^{j(xu + y\,v)}\ e^{j\gamma \int_0^t (b(x,y)\ cos\ (\omega t))\ dt}\ dxdy$$
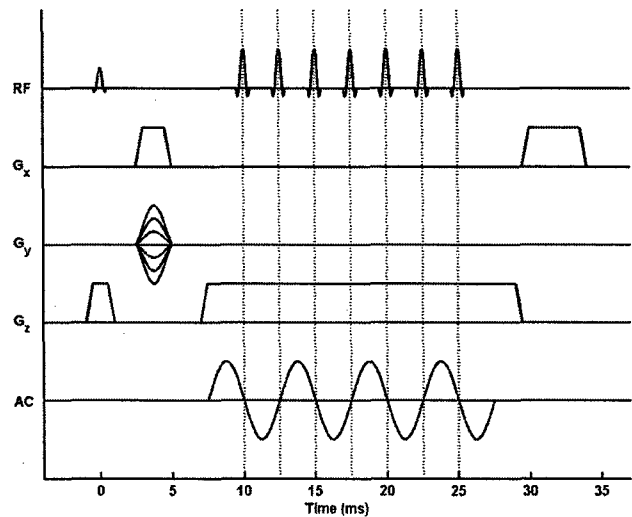
[1]

Figure 1: Timing diagram of the pulse sequence used in the MREIT experiments.

$M(x,y)$ is proportional to the density of protons within a voxel at coordinates (x,y). The phase angle $\theta_{(x,y)}$ accounts for all the constant phase terms including static field inhomogeneity and other hardware related phase delays. The gyromagnetic ratio is shown by γ, and u and v in this equation are called the "spatial frequencies". They are defined as $u=\gamma*G_x*T_{Gx}$ and $v=\gamma*G_y*T_{Gy}$, where T_{Gx} and T_{Gy} represent the duration of the gradient pulses Gx and Gy, respectively. Therefore, in the final image the accumulated total phase at a pixel at location (x,y) due to the magnetic field generated by injected currents is:

$$\varphi(x,y) = 4 \cdot \gamma \cdot N \cdot b(x,y) / \omega$$

[2]

where N is the number of cycles of injected current, $b(x,y)$ the amplitude of the z-component current-generated magnetic field at point (x,y), and ω the angular frequency of the injected current. Hence, measurement of this phase shift allows for calculation of the (z-component) magnetic field distribution.

During the experiments, the data was collected twice with opposite polarities of electric current, hence changing the polarity of current-generated magnetic field distribution. When resulting phase terms were subtracted, those coming from the static field inhomogeneities and delays in MRI hardware were eliminated, leaving only the terms caused by $b(x,y)$. To obtain the magnetic field distribution $b(x,y)$ from the acquired data, the MRI images were first reconstructed using the FFT. The resulting phase terms from the two sets of images were subtracted. Then, the magnetic field term was calculated using the expression given in Equation [2].

Hardware: An HP ESG-4400B signal generator produced the sine waves. These signals were synchronized to the

pulse sequence by a TTL pulse generated by the scanner computer. A transconductance amplifier was designed and built using three LM741 OPAMP circuits to convert the voltage from the signal generator into a current output. This circuit is described in detail in (28), which was replicated from (29). The output current was calibrated to 1ma/2V and an independent measurement of current was not used in the present study. The whole experimental setup is illustrated in Figure 2. MRRS console controls the whole experiment, which generates the pulse sequence, acquires the incoming data, and synchronizes the external units. After data collection, raw MRI data (k-space) was exported to another Pentium PC for off-line processing.
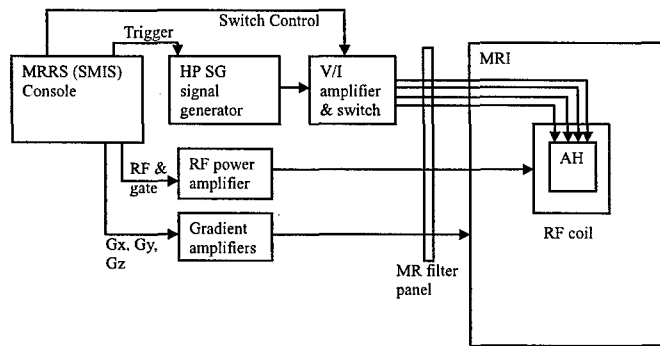
Figure 2: Schematic of the experimental setup. AH is the animal holder, which is placed inside the MRI RF coil.

Conductivity Image Reconstruction

Sensitivity Matrix Method: Since the relation between the conductivity distribution and the magnetic fields generated by the internal current distribution is nonlinear, one has to either employ iterative techniques or try to linearize around an initial value. In the presented study, the second approach was adopted, in which a linear relationship between the conductivity perturbations, $\Delta\sigma$, and magnetic field perturbations, ΔB, was assumed (16). This relationship is given in Equation [3] as:

$$\Delta B = S \cdot \Delta\sigma \qquad [3]$$

If there are n conductivity elements and m measurement points, then $\Delta\sigma$ is an $n \times 1$ vector, ΔB is an $m \times 1$ vector and the "sensitivity matrix" S is an $m \times n$ matrix. The entry of the sensitivity matrix at i^{th} row and j^{th} column denotes the change in the ith field measurement due to a small change in conductivity of the jth element.

In order to calculate the "sensitivity matrix" S one must solve the forward problem for a given conductivity distribution and current injection scheme. First, the initial magnetic field B_i is calculated from an initial estimate of conductivity (σ_i). Then, S is calculated by perturbing each element of σ_i one by one and finding the corresponding magnetic field distribution.

In the first step, the electric potential distribution $\phi(x,y,z)$ in the imaging slice is determined by solving the Poisson's equation with Neumann boundary value conditions. This problem is nonlinear in terms of conductivity since the electric potential itself is also conductivity dependent. The Finite Element Method (FEM) was used to calculate the distribution of the potential. Once ϕ is calculated, the electric field and current density distribution inside the imaging region may be found using the equations:

$$\vec{E} = -\nabla\phi$$
$$\vec{J} = \sigma \vec{E} \qquad [4]$$

The magnetic field generated by this ohmic current can be calculated by using Equation [4] and the Biot-Savart law. The differential magnetic field can be written in terms of the differential current element $I d\vec{l}$ as,

$$d\vec{B} = \frac{\mu_0 I}{4\pi}\left(\frac{d\vec{l} \times \vec{R}}{R^3}\right) \qquad [5]$$

where μ_0 is the permeability constant and $\vec{R}$ is the vector from the source point at (x', y', z') to the field point (x, y, z). The relationship between the current and magnetic field is linear and the total magnetic field can be obtained by integrating Equation [5] over all sources. Using Equations [4-5], the magnetic field can be calculated for an assumed conductivity distribution.

The sensitivity matrix can be calculated using either a numerical or a semi-analytical approach. In the numerical approach, each column of the sensitivity matrix is calculated separately by solving the forward problem by changing the conductivity of a single element. This approach requires the repetitive solution of the forward problem and increases the execution time. For faster reconstruction, the semi-analytical method was used for the calculation of the sensitivity matrix as explained in (20).

Once the sensitivity matrix S is calculated for certain geometry, the conductivity distribution can be approximated by,

$$\Delta\sigma = S^{-1} \cdot \Delta B \qquad [6]$$

Where $\Delta B = B_{meas} - B_i$; B_{meas} is the magnetic field measurements obtained from MRI and B_i is the initial value of the magnetic field corresponding to the initial conductivity distribution σ_i. The generalized inverse, S^{-1}, is found by using singular value decomposition (SVD). This method has been tested both by simulation and experimental phantom studies and shown that a good approximation to the relative conductivity distribution map can be obtained (16, 20).

Phantom Experiments

A series of phantom studies were conducted to test the spatial resolution and dynamic range of contrast for MREIT. Several agarose gel phantoms with different conductivity distributions were prepared for the tests. The gels were placed inside an acrylic cylinder with an inner diameter of 7cm and height of 1cm. The conductive gels consisted of 2% (g/100mL) agarose and varying concentrations of NaCl. During imaging, the axis of the cylinder was placed parallel to the z-axis (direction of the MRI magnetic field). Four electrodes made of copper foil, each 3mm wide, were placed at 0°, 90°, 180° and 270° along the inner wall and used to inject currents into the interior region. For each phantom, data were collected twice for two current injection schemes and used simultaneously in conductivity reconstruction. The first time, current was injected between the electrodes at 0° and 180°, and the second time between the ones at 90°, and 270°. In the preliminary studies conducted, it has been empirically verified that this scheme improves the sensitivity and spatial resolution compared to using a single pair of electrodes. In all phantom studies, current carrying wires were placed precisely in the z-direction to eliminate any contribution from the currents flowing in those wires. Wires were mounted on acrylic support beams for rigidity and several RF chokes and low pass filters were placed along these wires to suppress RF coupling.

For contrast studies, a 16mm diameter inner disk of gel surrounded by a background of 1% NaCl was used. Two experiments were carried out with two similar contrast phantoms, where the inner disk contained either 4% or 10% NaCl. In the preliminary tests, it has also been experimentally verified that conductance scales sufficiently linearly with NaCl concentration. Therefore, the conductivity contrast values were approximately 1:4 and 1:10, respectively.

To study spatial resolution, two different phantoms were imaged. The first phantom was prepared by placing two hollow nylon disks (each 16mm in diameter) inside the larger disk. They were separated by 17mm center to center. The nylon shells acted as insulators, and each small disk was filled with the same gel as the surrounding background. The second phantom was prepared with the same geometry as the first one but this time the inner disks were agar gels with a conductivity ten times higher than the background.

For each phantom configuration, two separate data sets were collected by injecting 6 cycles of 2mA or 4mA (rms) 200Hz current into the phantom. All data were collected using the previously outlined pulse sequence with the following parameters: TR=500ms, TE=40ms, slice thickness=1cm, FOV=10cm, data matrix 64 × 64 and NEX=8. A single slice was collected for each experiment. The z-component of current-generated magnetic field distributions were calculated from the resulting data and the conductivity distributions computed using the method outlined above.

Effect of Initial Conductivity Estimate

As described in the methods section, conductivity reconstruction requires an initial estimate of conductivity distribution. We performed simulation studies to investigate the effect of this initial estimate on reconstructed conductivity and contrast. Four cylindrical phantoms were generated, each with a small disc inside, which was placed off-center. All four phantoms were generated with a background conductivity of 0.002S/cm and the conductivity of the small disk was assigned either 0.5, 2, 4 or 10 times the background conductivity.

Each of the four phantom data were reconstructed three times with uniformly distributed initial conductivity estimates of 0.001S/cm, 0.002S/cm and 0.004S/cm, respectively. Singular values below 1% were truncated and 1089 nodes and 2048 first order triangular elements were used in all finite element models used in reconstructions.

Animal Experiments

An MREIT experiment was also performed for *in vivo* impedance imaging of a tumor-bearing rat. For this purpose, a special animal holder was prepared from acrylic sheets. This holder helped keep the animal stationary during imaging. It also allowed for the placement of the electrodes in consistent positions for longitudinal studies. Electrodes were placed on acrylic hollow tubes filled with CuSO4 solution to detect the electrode positions precisely in the images. Initial experience has shown that the precise localization of electrode positions is essential for accurate reconstruction of impedance images. Current carrying wires ran along these tubes, which were in z-direction. This is essential to minimize interference from the magnetic fields generated by current in the wires. Prior to imaging, the animal was anesthetized by IV injection of ketamine and xylazine and then placed inside the holder. The electrodes were covered with a thin layer of conductive gel to provide good electrical contact. The skin areas of contact were shaved for better conductance.

An anatomical image was collected using FSE sequence prior to the MREIT images. A single slice with 6mm thickness was collected from the same anatomical location as the MREIT image. The data matrix was 256 × 256, FOV=10cm, TR=4s, TE=20ms/100ms NEX=4. MR-EIT images were collected using the previously outlined pulse sequence with TR=500ms, TE=30ms, NEX=8 (signal averages), 64 × 64 data matrix, FOV=10cm, slice thickness=6mm, with an AC current of 1mA peak, 200Hz, 4 cycles.
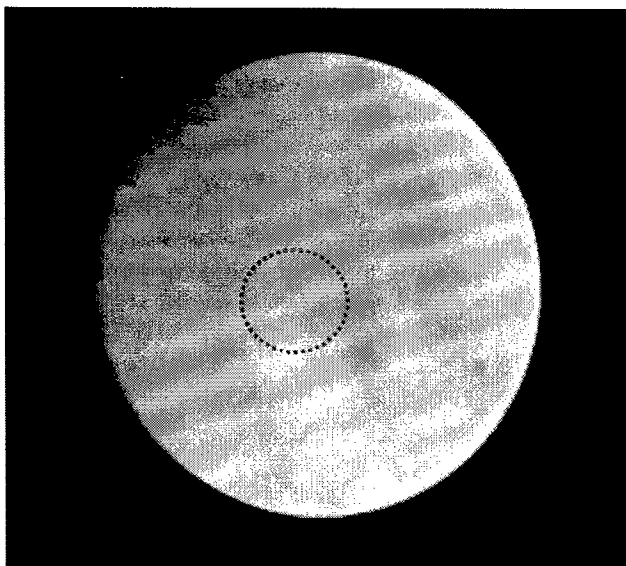
Figure 3a: Spin-Echo image of 1:4 contrast phantom. The higher conductivity region is marked with red dashed lines and it is barely distinguishable in the MR image.
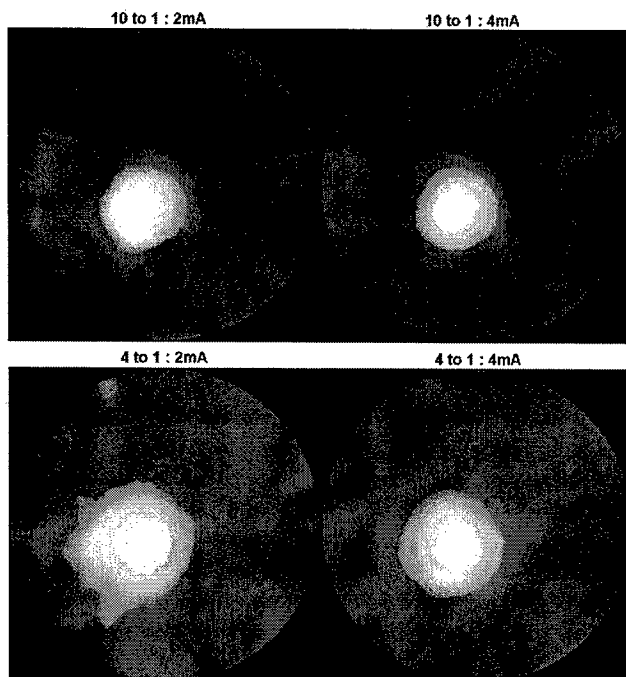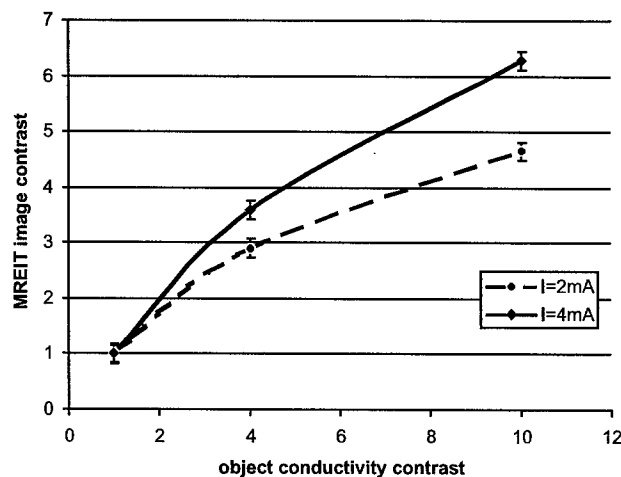

Figure 3c: Plots of *reconstructed conductivity ratio* versus *actual conductivity ratio* obtained from MREIT images. Plots are given for both of the injected current amplitudes. Error bars are also included in these plots.
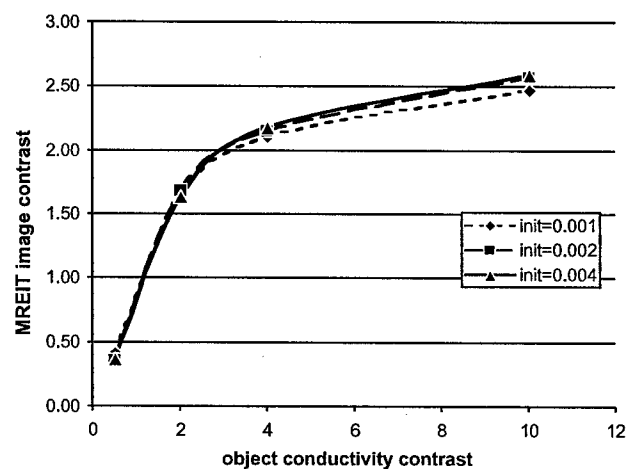

Figure 3b: Conductivity images of 1:10 contrast (top row) and 1:4 contrast (bottom row) with 2mA and 4mA current injection cases.

Figure 3d: Plots of *reconstructed conductivity ratio* versus *actual conductivity ratio* in the phantom data used in MREIT simulations. Three plots are given for three different initial conductivity estimates of 0.001, 0.002 and 0.004S/cm. Actual background conductivity was given as 0.002S/cm.

Table I

Mean and standard deviation of relative conductivity (σ_{ir}, σ_{or}) values in contrast phantoms calculated by the MREIT method. Results are reported for both injected current amplitudes.

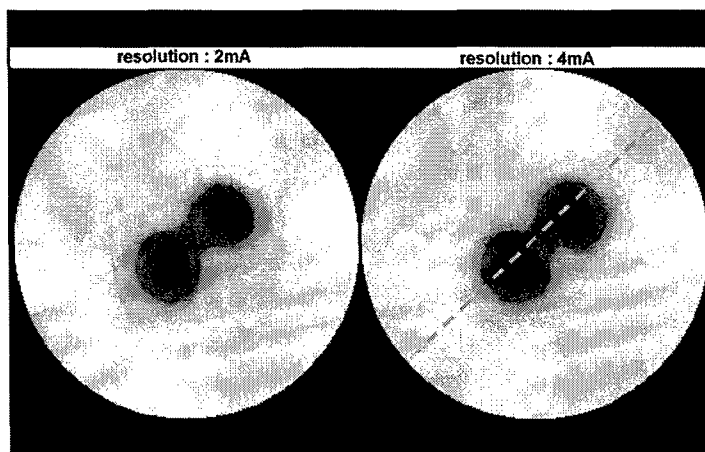|	$\sigma_o{:}\sigma_i = 1{:}4$ phantom (m±std)		$\sigma_o{:}\sigma_i = 1{:}10$ phantom (m±std)	
	I=2mA	I=4mA	I=2mA	I=4mA
Inside small disk (σ_{ir})	235.4±10.5	229.6±18.4	233.4±15.4	226.6±21.2
Background (σ_{or})	81.2±18.3	63.8±14.7	50.1±17.9	36.1±12.3

Figure 4a: Conductivity images of resolution phantom with insulating discs. Both, 2mA and 4mA current injection cases were shown. Small, dark circular areas show high resistance compartments (insulating disks).
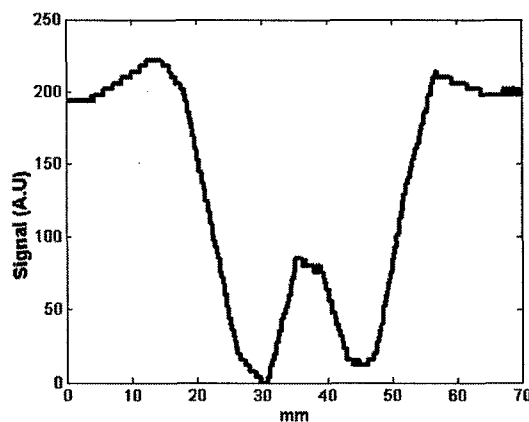

Figure 4b: A profile taken diagonally from the conductivity image of the first resolution phantom going through the centers of the small disks. This profile is given for the 4mA current injection case and the location is shown with blue dashed line in Figure 4a.
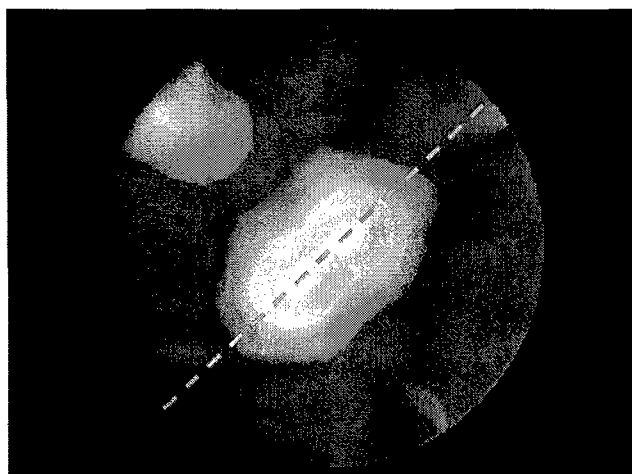

Figure 4c: Conductivity images of resolution phantom with high conductivity discs. Only the 4mA current injection case is shown. Yellow-white circular areas show low resistance compartments.
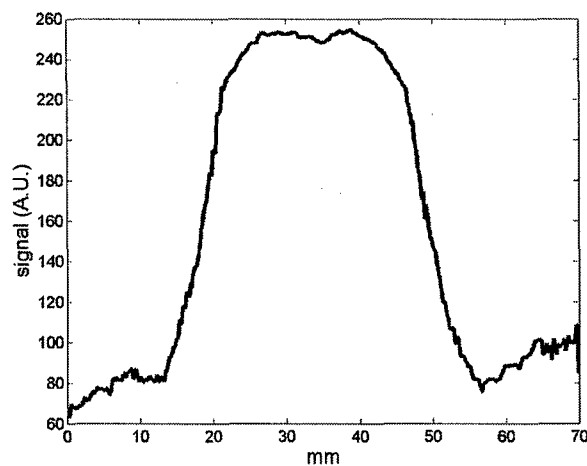

Figure 4d: A profile taken diagonally from the conductivity image of the second resolution phantom shown in Figure 4c.
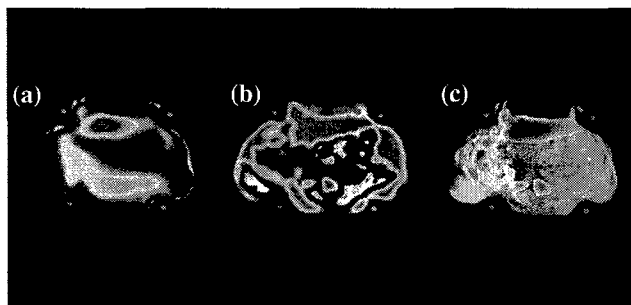

Figure 5: Axial slices from an SD rat inoculated with a R3230 AC tumor showing: (a) Conductivity; (b) CE-MRI; and (c) spatial correlation of CE-MRI and MREIT. The tumor had spread to multiple foci surrounding the body. In (a), red shows high conductivity and blue shows low conductivity regions; whereas red regions in (b) shows enhancement by Gd-DTPA. Areas that have both high conductivity and also enhanced by contrast agent are shown in hot colors in (c).
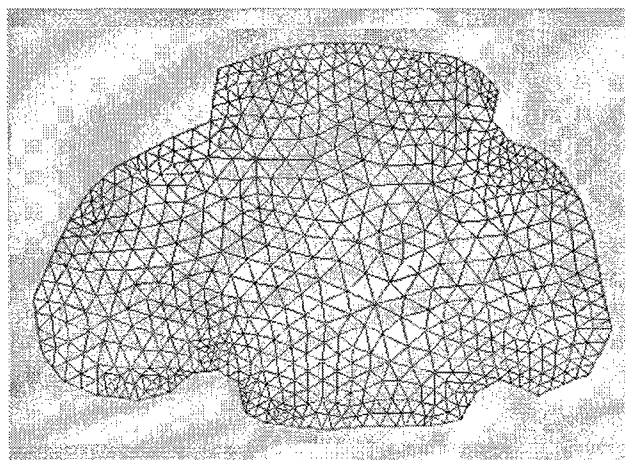

Figure 5d: FEM mesh constructed from the anatomical MR Image.

Contrast enhanced MR images were also collected (CE-MRI) using Gd-DTPA, which is a well-established method to detect malignant tissues. Since vascular growth is greatly enhanced in tumor structures, contrast agent uptake of tumor sites increases with respect to normal tissues. In addition to that, interstitial compartment in tumors are large compared to normal structures, so the wash-out of contrast agent is also slower in tumors. Therefore, if two images are collected, one pre-contrast and the other post-contrast, the difference image yields enhanced pixel intensity in the areas of tumor growth. In this study, the goal was to verify the potential of MR-EIT to detect tumors. Contrast enhanced images were collected using a GE sequence with a 64 × 64 data matrix, FOV=10cm, 6mm slice thickness, TR=150ms, TE=5ms, and 45° flip angle. One pre-contrast image was acquired before Gd-DTPA injection and a post-contrast image was collected 3 minutes after injection.

Results

Conductivity images were reconstructed using the method outlined in the *Methods* section. In the calculation of the inverse of S using SVD, the highest 200 singular values were used and the rest were truncated to minimize noise while preserving essential information. This value was also determined experimentally to be an optimum level for truncation. In the FEM mesh, 512 triangular elements were used.

Impedance Contrast Phantoms

Figure 3a illustrates the standard spin-echo MRI image acquired from the contrast phantom (with 1:4 conductivity contrast). As seen in the Figure, it is difficult to distinguish the two compartments in the MRI image. The top row in Figure 3b shows conductivity images obtained from the 1:10 contrast phantom with two separate current amplitudes. Similarly, the bottom row of Figure 3b shows conductivity image of the 1:4 contrast phantom. Higher conductivity regions are greatly enhanced in the resulting images. The means of the reconstructed relative conductivity values in the two compartments inside the contrast phantoms were calculated and given in Table I.

Figure 3c shows the relationship between relative object conductivity values and relative MREIT image conductivity values as measured from the images given in Figure 3b (and Table I). Since the background conductivity is kept the same for 1:4 and 1:10 contrast phantoms, all conductivity values reported in Table I were normalized by their corresponding background values (σ_{or}) for this graph. Thus, the conductivity image contrast is obtained by dividing the mean conductivity in small disk (σ_{ir}) by the background mean value (σ_{or}). Using these measurements, the relative changes in object conductivity and corresponding conductivity contrast

in the MREIT images were plotted. The plots are given for both 2mA and 4mA injected current cases. A non-linear relationship is observed in these plots. Moreover, the difference between the two curves was statistically significant.

Effect of Initial Conductivity Estimate on Contrast

The reconstructed images in simulation studies were analyzed to assess the effect of initial estimate in conductivity image contrast. Mean values in the background and inner disc were calculated for each of the generated 1:0.5, 1:2, 1:4 and 1:10 contrast phantoms. Those values are calculated for each of the three different initial estimates of 0.001, 0.002 and 0.004S/cm. *Reconstructed conductivity ratio* is defined as the mean value of the inner disk divided by the mean value of the background in the reconstructed images. For each of the three initial estimates, a graph of *actual conductivity ratio* versus *reconstructed conductivity ratio* was plotted in Figure 3d.

Spatial Resolution Phantoms

Figure 4a shows the conductivity image of the "spatial resolution phantom" with two identical nylon disks. The results of two experiments with 2mA and 4mA current injections are given in this Figure. The gradually decreasing distance between the two small disks was used to assess the spatial resolution capability of conductivity images. A cross sectional profile taken diagonally from Figure 4a is shown in Figure 4b. This profile was taken from a cut that passed through the centers of the small disks. Even though the contrast was somewhat reduced due to low-pass filtering of the point-spread function, the 1mm separation could still be observed. On the other hand, the conductivity phantom with ten times higher conductivity does not provide the same precision of detection capability (Figure 4c). The 1mm separation is hardly distinguishable in this figure.

In vivo *Imaging*

The first step in animal imaging is the construction of the finite element mesh using an anatomical high resolution MRI image. The FEM mesh shown in Figure 5d consists of 702 nodes and 1268 first order triangular elements. Exact electrode locations are found using the markers in the animal setup and used for the boundary condition determination. The relative conductivity distribution was computed as described above and overlaid on the anatomical image (Figure 5a). The resulting images show the higher conductivity regions with high contrast. Similarly, the contrast enhancement by Gd-DTPA is illustrated in Figure 5b. To investigate how the two images spatially correlate, another image was generated by masking the CE-MRI image with the MREIT image regions that have conductivity values in the upper one-thirds of the full range. Figure 5c shows regions that have high conductivity and also enhanced by Gd-DTPA.

Discussion

In this preliminary study, the potential of the MREIT method for obtaining *in vivo* conductivity information with good spatial resolution and sensitivity was demonstrated, which may be helpful in identifying malignant tumors.

In the results presented here, a fixed frequency of 200Hz was used for the applied electrical currents. This choice was based on previous studies that investigated electrical properties of tumors (7). Those studies have reported that a higher conductivity contrast was obtained with the application of 200Hz currents.

In contrast phantom tests, conductivity ratios of 1:4 and 1:10 were used. The method presented here clearly detected these conductivity perturbations in the objects. Based on the range of conductivity changes of malignancies compared to those of benign or healthy tissues that were reported in the literature (1), MREIT should offer sufficient sensitivity for the detection of malignancies. Although the minimum detectable conductivity perturbation by MREIT has not been tested, from the results presented, it may be anticipated that much smaller changes could also be detected.

Since the reconstruction method used here is based on the linearity assumption between conductivity perturbations and measured magnetic fields, it only gives precise relative conductivity measurements for small conductivity perturbations within the object (or body). In the results presented here, the ratio of conductivity values measured in various compartments in the reconstructed images did not reflect the actual conductivity contrast. Since relatively large conductivity changes were used in the phantoms, it was observed that the conductivity contrast in the images was lower than the actual ratios due to the nonlinear nature of the actual relationship. The non-linear relationship between conductivity perturbations in the object versus perturbations in reconstructed EIT images was studied in detail by Ider *et al.* (27). These problems, arising from the nonlinearity of reconstruction method, can be minimized by using iterative reconstruction techniques with regularization. One such technique called the *weighted regularized least square method* (WRLSM) was used by Oh *et al.* (30) to reconstruct conductivity images using MRI. Although they applied this method to *harmonic Bz algorithm*, it can be easily adopted to our reconstruction technique. *Harmonic Bz algorithm* requires the second partial derivatives of the magnetic field Bz ($\nabla^2 Bz$), therefore, it is vulnerable to the noise in the Bz measurements. Spatial dependence of accuracy was observed in Oh's study, where the two profiles from different sections of conductivity images revealed different accuracy with respect to the true conductivity profiles. Moreover, they have used significantly higher current amplitude of 26mA, compared to the val-

ues of 2 and 4mA used in the presented study. One advantage of our reconstruction technique is that it is less vulnerable to noise compared to the *harmonic Bz* algorithm, because of the fact that it does not require derivatives of Bz. Therefore, an iterative WRLSM technique is expected to improve accuracy of relative conductivity images obtained in our studies. Our group is currently working on the implementation of such a technique. In addition to that, it can also be observed that the contrast in the conductivity images decreased when the amplitude of the current was decreased from 4 to 2mA. Since the non-linear relationship between magnetic field distribution and conductivity values is assumed to be linear in the sensitivity matrix method, the degree of deviation from linearity will vary with changing current amplitude. As seen in the Figure, the curve with 2mA current amplitude is slightly more linear compared to the 4mA current injection case but with reduced slope, *i.e.*, reduced contrast. This aspect could be an important consideration in longitudinal studies where the change in conductivity in a tumor is investigated over time.

Simulation studies have shown that the relative conductivity contrast in reconstructed images is also dependent on the initial conductivity estimate. Slight deviations in curves shown in Figure 3d were observed within the range of initial values tested. Therefore, the initial estimate of conductivity in sensitivity matrix reconstruction will have an impact on the resultant image contrast.

Two simple phantoms were prepared, where the separation between two closely separated non-conductive or highly conductive disks were used to assess resolution. It was found that the closest distance of 1mm was still detectable in the images where non-conducting disks were used. On the other hand, the 1mm separation was hardly distinguishable in the phantom with highly conductive disks. Therefore, the relative conductivity of inner structures plays an important role in the resolution, as expected. Current density is an important factor that determines sensitivity in this imaging technique. High current density in a particular area will increase sensitivity in that area. Thus, in the non-conducting object case, there will be high current density between the two insulators, whereas, in the high-conductivity object case, most of the current density will be concentrated inside the relatively large objects and suppress the perturbation of small separation. Moreover, a certain amount of diffusion between the high-conductivity objects and the low-conductivity separation can be expected, which will adversely affect the resolution. To minimize that effect, images are collected immediately after the phantom preparation. For better assessment of resolution, diffusion has to be taken into account. Similarly, it may be expected that the detectability of the object separation will also be affected by the size of the inner disks. Construction of

sophisticated high-resolution phantoms with agarose gel is a mechanically challenging task due to the lack of rigidity in the gel structure. Small structures can easily melt and blend into each other making boundaries somewhat ambiguous. Although more complicated phantoms could be built with different materials to investigate the spatial resolution of the method, these two simple phantoms illustrate how well the separation between objects of different conductivity could be resolved. Generally, a high contrast object is required to assess the spatial resolution of an imaging technique, since it is affected less by noise; therefore, the test with insulators appears to be a better assessment of the resolution in the presented study.

Similarly, conductivity images collected from animals *in vivo* showed significantly increased conductivity in tumor areas. Tumor location was identified by contrast enhanced MRI. It is seen from these results that there is high correlation between the conductivity images and contrast enhanced MR images. Although they do not completely overlap, this is expected because the two methods emphasize different properties of tumors. For example, edema will most likely show high conductivity but will not show signal enhancement with the CE-MRI. To exclude edematous regions from the conductivity images, one can use T2 weighted sequences that highlights edema. In this preliminary experiment, an animal with a large tumor size was imaged, which was available at the time. As seen in the CE-MRI images, the tumor had spread into several foci that encircled the animal's trunk. In large tumors, various compartments like edema, necrosis and viable tumor cells exist and their conductivity and contrast agent enhancement will be different. Currently, a longitudinal study is planned to observe changes in conductivity as well as Gd-DTPA based contrast enhancement in tumor structures as the tumor grows. The CE-MRI will be used to verify the MREIT results *in vivo*. At the end of the study, tumors will be excised and undergo histologic analysis. Contrast enhanced and T2 weighted images together with the MREIT maps will allow for the assessment of how conductivity correlates with different compartments in tumors. The positions and numbers of electrodes could be another factor that may confound the detection of some low conductivity structures close to surface. The effects of electrode placement will also be investigated in future studies.

In all phantom studies, as well as *in vivo* experiments, the current carrying wires were placed precisely in the z-direction with acrylic support beams. Those wires were attached to the electrodes without any bends. Therefore, the magnetic fields generated by the currents in these lead wires would have mainly B_x and B_y components and B_z will be negligible. Therefore, any significant contribution from the currents in the lead wires to the B_z measurements is not expected.

In general, currents flowing in an object generate a 3D magnetic field. The currents flowing inside an imaging slice generate a magnetic field that has only a component, which is perpendicular to the plane of the slice. In this preliminary study, the magnetic fields generated by currents outside the imaging slice were ignored, reducing the reconstruction to 2D. Since most of the current flow will be concentrated between the electrodes, this approximation was deemed to be adequate for the pilot studies. Currently, 3D reconstruction methods are being be developed in our laboratory that will account for such out-of-slice effects.

Acknowledgements

References

1. Surowiec, A. J., Stuchly, S. S., Barr, J. R., and Swarup, A. Dielectric Properties of Breast Carcinoma and the Surrounding Tissues. *IEEE Trans. on BME 35* 257-263 (1988).
2. Elmore, J. G., Barton, M. B., Moceri, V. M., Polk, S., Arena, P. J., and Fletcher, S. W. Ten-year Risk of False Positive Screening Mammograms and Clinical Breast Examinations. *The New England Journal of Medicine 338*, 1089-1096 (1998).
3. Christiansen, C. L., Wang, F., Barton, M. B., Kreuter, W., Elmore, J. G., Gelfand, A. E., and Fletcher, W. Predicting the Cumulative Risk of False-Positive Mammograms. *Journal of the National Cancer Institute 92*, 1657-1666 (2000).
4. Elmore, J. G., Miglioretti, D. L., Reisch, L. M., Barton, M. B., Kreuter, W., Christiansen, C. L., and Fletcher, S. W. Screening Mammograms by Community Radiologists: Variability in False-Positive Rates. *Journal of the National Cancer Institute 94*, 1373-1380 (2002).
5. Moore, S. K. Better Breast Cancer Detection. *IEEE Spectrum 38*, 50-54 (2001).
6. Coons, T. A. MRI's Role in Assessing and Managing Breast Disease. *Radiological Technology 67*, 311-336 (1996).
7. Malich, A., Boehm, T., Facius, M., Freesmeyer, M. G., Fleck, M., Anderson, R., and Kaiser, W. A. Differentiation of Mammographically Suspicious Lesions: Evaluation of Breast Ultrasound, MRI Mammography and Electrical Impedance Scanning as Adjunctive Technologies in Breast Cancer Detection. *Clinical Radiolody 56*, 278-283 (2001).
8. Boone, K., Barber, D. and Brown, B. Imaging with Electricity: Report of the European Concerted Action on Impedance Tomography. *Journal of Medical Engineering and Technology 21*, 201-232 (1997).
9. Cherepenin, V., Karpov, A., Korjenevsky, A., Kornienko, V., Mazaletskaya, A., Mazourov, D., and Meister, D. A 3D Electrical Impedance Tomography (EIT) System for Breast Cancer Detection. *Physiological Measurement 22*, 9-18 (2001).
10. Estrela da Silva, J., Marques de Sá, J. P., and Jossinet, J., Classification of Breast Tissue by Electrical Impedance Spectroscopy. *Medical and Biological Engineering and Computing 38*, 26-30 (2000).
11. Kerner, T. E., Paulsen, K. D., Hartov, A., Soho, S. K., and Poplack, S. P. Electrical Impedance Spectroscopy of the Breast: Clinical Imaging Results in 26 Subjects. *IEEE Trans. on Medical Imaging 21*, 638-645 (2002).
12. Malich, A., Fritsch, T., Anderson, R., Boehm, T., Freesmeyer, M. G., Fleck, M., and Kaiser, W. A. Electrical Impedance Scanning for Classifying Suspicious Breast Lesions: First Results. *Eur. Radiol. 10*, 1555-1561 (2000).

13. Malich, A., Fritsch, T., Mauch, C., Boehm, T., Freesmeyer, M., Fleck, M., Anderson, R., and Kaiser, W. A. Electrical Impedance Scanning: A New Technique in the Diagnosis of Lymph Nodes in Which Malignancy Suspected on Ultrasound. *The British Journal of Radiology 74*, 42-47 (2001).

14. Malich, A., Boehm, T., Facius, M., Freessmeyer, M., Fleck, M., Anderson, R., and Kaiser, W. A. Additional Value of Electrical Impedance Scanning: Experience of 240 Histologically-proven Breast Lesions. *European Journal of Cancer 37*, 2324-2330 (2001).

15. Assenheimer, M., Laver-Mokovitz, O., Malonek, D., Manor, D., Nahaliel, U., Nitzan, R., and Saad, A. The T-SCAN™ Technology: Electrical Impedance as a Diagnostic Tool for Breast Cancer Detection. *Physiological Measurement 22*, 1-8 (2001).

16. Ider Y. Z. and Birgul, O. Use of the Magnetic Field Generated by the Internal Distribution of Injected Currents for Electrical Impedance Tomography (MR-EIT). *Elektrik, Turkish Journal of Electrical Engineering and Computer Sciences 6*, 215-225 (1998).

17. Birgul, O., Eyuboglu, M., and Ider, Y. Z. A New Technique for High Resolution Absolute Conductivity Imaging Using Magnetic Resonance-Electrical Impedance Tomography (MR-EIT). *Proceedings of SPIE – The International Society for Optical Engineering, Medical Imaging 4320*, 880-888 (2001).

18. Khang, H. S., Lee, B. I., Oh, S. H., Woo, E. J., Lee, S. Y., Cho, M. H., Kwon, O., Yoon, J. R., and Seo, J. K. J-Substitution Algorithm in Magnetic Resonance Electrical Impedance Tomography (MREIT): Phantom Experiment for Static Resistivity Images. *IEEE Trans. on Medical Imaging 21*, 695-702 (2002).

19. Birgul, O., Eyuboglu, B. M., and Ider, Y. Z. Current Constrained Voltage Scaled Reconstruction (CCVSR) Algorithm for MR-EIT and its Performance with Different Probing Current Patterns. *Physics in Medicine and Biology 48*, 653-671 (2003).

20. Birgul, O., Eyuboglu, B. M., and Ider, Y. Z. Experimental Results for 2D Magnetic Resonance–electrical Impedance Tomography (MR-EIT) Using Magnetic Flux Density in One Direction. *Physics in Medicine and Biology 48*, 3485-3504 (2003).

21. Oh, S. H., Han, J. Y., Lee, S. Y., Cho, M. H., Lee, B. I., and Woo, E. J. Electrical Conductivity Imaging by Magnetic Resonance Electrical Impedance Tomography (MREIT). *Magnetic Resonance in Medicine 50*, 875-878 (2003).

22. Scott, G. C., Joy, M. L. G., Armstrong, R. L., and Henkelman, R. M. Measurement of Non-uniform Current Density by Magnetic Resonance. *IEEE Trans on Medical Imaging 10*, 362-374 (1991).

23. Ider, Y. Z. and Muftuler, L. M. Measurement of AC Magnetic Field Distribution using Magnetic Resonance Imaging. *IEEE Trans. on Medical Imaging 16*, 617-622 (1997).

24. Mikac, U., Demsar, F., Beravs, K., and Sersa, I. Magnetic Resonance Imaging of Alternating Electric Currents. *Magnetic Resonance Imaging 19*, 845-856 (2001).

25. Scott, G. C., Joy, M. L. G., Armstrong, R. L., and Henkelman, R. M. Electromagnetic Considerations for RF Current Density Imaging. *IEEE Trans. on Medical Imaging 14*, 515-524 (1995).

26. Glickman, Y. A., Filo, O., Nachaliel, U., Lenington, S., Amin-Spector, S., Ginor, R. Novel EIS Postprocessing Algorithm for Breast Cancer Diagnosis. *IEEE Trans. on Medical Imaging 21*, 710-712 (2002).

27. Ider, Y. Z., Eyuboglu, B. M., Kuzuoglu. M., Leblebicioglu, K., Baysal, U., Caglar, B. K., and Birgul, O. A Method for Comparative Evaluation of EIT Algorithms Using a Standard Data Set. *Physiol. Meas. 16*, A227-A236 (1995).

28. Baumann, B. B., Wozny, D. R., Kelly, S. K., Meno, F. M. The Electrical Conductivity of Human Cerebrospinal Fluid at Body Temperature. *IEEE Trans. BME 44*, 220-223 (1997).

29. Ackmann, J. J. Complex Bioelectric Impedance Measurement System for the Frequency Range from 5 Hz to 1MHz. *Annl. Biomed. Eng. 21*, 135-146 (1993).

30. Oh, S. H., Lee, B. I., Woo, E. J., Lee, S. Y., Cho, M. H., Kwon, O., Seo, J. K. Conductivity and Current Density Image Reconstruction using *Harmonic Bz Algorithm* in Magnetic Resonance Electrical Impedance Tomography. *Phys. Med. Biol. 48*, 3101-3116 (2003).

Assessment of the Efficacy of Electrical Impedance Imaging Using MRI

M. Hamamura[1], L. T. Muftuler[1], O. Birgul[1], O. Nalcioglu[1]

[1]John Tu & Thomas Yuen Center for Functional Onco-Imaging, University of California, Irvine, CA, United States

Synopsis

In this study, we carried out a set of experiments to measure electrical impedance changes in phantoms prepared to assess the spatial resolution and contrast resolution of an MRI based impedance imaging method. A special reconstruction method is proposed which utilizes only one component of the magnetic field. Initial results show that the method can resolve impedance perturbations of several mm in size. It has also been shown that impedance ratios of 4:1 can be resolved clearly.

Purpose

It has been shown that the electrical impedance of malignancies is 20-40 times lower than healthy tissues and benign formations [*Malich A. et al, Eur. Radiol. 10: 1555-1561 (2000)*]. Therefore, in-vivo impedance imaging of suspicious lesions could aid in diagnosis of malignant tumors. MRI based impedance imaging is a novel method. In this method, weak electrical currents are injected into the tissue and the resulting perturbations in magnetic field encoded into the phase of MRI images are measured. In this study, we did phantom tests to assess the efficacy of the method before in-vivo applications.

Methods

Sinusoidal current is injected into an object and the resulting magnetic fields are measured using a modified spin-echo sequence (Figure 1) [*Mikac U. et al, MRI 19: 845 856 (2001)*]. The component of current-generated magnetic field parallel to the main static field (z-component) produces a phase shift. By synchronizing successive π pulses to half cycles of the current, this phase shift accumulates and is given in the final image as $\varphi(\mathbf{r}) = 4 \cdot \gamma \cdot N \cdot b(\mathbf{r}) / \omega$, where γ is the gyromagnetic ratio, N the number of cycles of injected current, $b(\mathbf{r})$ the amplitude of z-component current-generated magnetic field at point $\mathbf{r}$, and ω the angular frequency of the injected current. Hence, measurement of this phase shift allows for calculation of the (z-component) magnetic field distribution.

Figure 1

A linear approximation $\Delta B(\mathbf{r}) = S(\mathbf{r}, \mathbf{r}') \Delta\sigma(\mathbf{r}')$ is assumed, where $\Delta B(\mathbf{r})$ is the change in magnetic field at point $\mathbf{r}$ for a given current injection scheme resulting from a change $\Delta\sigma(\mathbf{r}')$ in the conductivity at point $\mathbf{r}'$. To compute S, the Finite Element Method (FEM) is utilized, whereby the object domain is discretized and S becomes a 'sensitivity' matrix. The matrix component S_{ij} is the change in magnetic field ∂B_i of element i with respect to a change in the conductivity $\partial\sigma_j$ of element j. An initial conductivity distribution σ_0 is assumed (e.g. uniform conductivity), the conductivity of a given element j perturbed by $\Delta\sigma_j$, the resulting ΔB calculated by the FEM, and matrix components approximated as $S_{ij} = \Delta B_i / \Delta\sigma_j$. The linear approximation can be inverted to yield $\Delta\sigma = \sigma_{final} - \sigma_{initial} = S^{-1} \Delta B = S^{-1} (B_{final} - B_{initial})$, where $\sigma_{initial}$ is the assumed initial (uniform) conductivity distribution, $B_{initial}$ the magnetic field distribution given $\sigma_{initial}$ and solved using the FEM, σ_{final} the actual conductivity distribution, B_{final} the MRI measured magnetic field distribution, and S^{-1} a truncated pseudoinverse calculated using singular value decomposition. Hence, the conductivity distribution of an object can be computed as $\sigma_{final} = S^{-1} (B_{final} - B_{initial}) + \sigma_{initial}$.

The previously outlined method was tested using several agarose gel phantoms. A hollow disk of acrylic with an inner diameter of 7cm and thickness of 1cm was filled with a conductive gel of 2% (g/100mL) agarose, 4mM CuSO4, and varying concentrations of NaCl. The plane of the disk was placed perpendicular to the z-axis. 4 electrodes each 5mm wide were placed equidistant along the inner wall and used to inject currents into the interior region. For each phantom, data was collected for different current injection schemes and used simultaneously in conductivity reconstruction.

Results

For a 'contrast' phantom, a 1cm diameter disk surrounded by a background of 1% NaCl was used (Figure 2a). The disk contained 10% NaCl in one experiment and 4% NaCl in another. 4 cycles of 10mA (rms) 200Hz current were injected into the phantom using the previously outlined pulse sequence with the parameters TR=500ms, TE=30ms, and NEX=4. The z-component current-generated magnetic field distribution was calculated from the resulting data and the conductivity distribution computed (Figures 2c&d). The resulting images clearly show the higher conductivity region, which is difficult to distinguish in the standard spin-echo proton density image (Figure 2b).

For a 'resolution' phantom, two hollow nylon disks each 8mm in diameter were separated by 2mm (Figure 2e). The nylon shells acted as insulators, and each small disk was filled with the same gel as the surrounding background. Injecting 4 cycles of 15mA (rms) 200Hz current and using the parameters TR=500ms, TE=30ms, and NEX=8, the z-component current-generated magnetic field distribution was computed and the conductivity distribution reconstructed (Figure 2f).

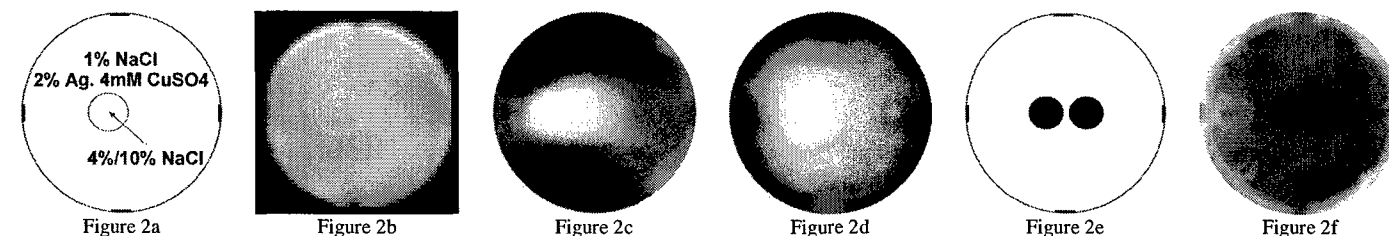| Figure 2a | Figure 2b | Figure 2c | Figure 2d | Figure 2e | Figure 2f |

Figure 2. (a) schematic of the contrast phantom; (b) MRI image; (c) 10:1 impedance contrast; (d) 4:1 impedance contrast; (e) schematic of the spatial resolution phantom; (f) spatial resolution image

Discussion

In this preliminary study, we have shown that MRI based impedance imaging can be used to analyze structures that may not reveal contrast in MRI images (Figure 2b) but are clearly distinguishable in impedance images (Figures 2c&d). It was also shown that the method clearly resolves impedance perturbations with a 4:1 ratio and a size of 1-2mm. We have not yet tested the minimum limit of contrast ratio, but these results suggest that much lower impedance contrasts can be resolved. As the next step, we have also applied this method to live animals with malignancies. The result of that study is being submitted concurrently.

MR-EIT of Malignant Tumors in Rats

O. Birgul[1], L. T. Muftuler[1], M. Hamamura[1], O. Nalcioglu[1]

[1]University of California, Irvine, CA, United States

Synopsis

In this study, we performed MR based Electrical Impedance Tomography (MR-EIT) on a laboratory rat with a malignant lesion. Images of impedance distribution were obtained using a pulse sequence that is sensitive to perturbations in magnetic flux density that are induced by the electrical currents injected to the animal using electrodes. Unlike previous methods to acquire current density images, our reconstruction method does not require rotation of the animal in the magnet. High impedance distribution in the muscle region and low impedance distribution in the tumor were observed, that are in accord with the literature.

Purpose

It is observed that the electrical impedance of malignant lesions is 20-40 times lower than the healthy tissues and benign lesions [*Malich A. et al, Eur. Radiol. 10: 1555-1561 (2000)*]. The goal of this study was to acquire in-vivo impedance images from live animals with tumors to assess the diagnostic potential of MR-EIT.

Methods

The magnetic flux density generated due to injected AC currents can be measured using MRI with a specifically designed pulse sequence [*Mikac U. et al, MRI 19: 845-856 (2001)*]. The details of the pulse sequence are given in another abstract submitted concurrently. Only the component of the magnetic flux density in the direction of main field (z-component) introduces additional phase. Once the magnetic flux density is calculated from the phase images, inverse problem of calculating conductivity distribution from magnetic flux density can be solved. This method is named as magnetic resonance electrical impedance tomography (MR-EIT). A sensitivity matrix based image reconstruction algorithm for MR-EIT is implemented. In this approach, the magnetic flux density distribution is linearized around an initial conductivity distribution, $\sigma_{initial}$, and the relation between conductivity and magnetic flux density perturbations is written as $\Delta B = S \Delta\sigma$. Note that ΔB contains the magnetic flux density values in z-direction only. The problem is formulated in two dimensions. The sensitivity matrix, S, is calculated analytically for a given $\sigma_{initial}$ and 2D Finite Element Method (FEM) mesh. For objects with arbitrary shape, the boundary information is extracted from typical spin echo image and the FEM mesh is generated using MATLAB® Partial Differential Equation toolbox for the given boundary information. The inverse problem is solved as $\Delta\sigma = \sigma_{desired} - \sigma_{initial} = S^{-1} (B_{measured} - B_{initial})$ where S^{-1} is the truncated pseudo inverse calculated using singular value decomposition. A uniform conductivity distribution is assumed as the initial and the corresponding $B_{initial}$ and S are calculated. $B_{initial}$ is independent of the conductivity value as long as uniform conductivity is used. In order to find conductivity distribution uniquely, at least two different current distributions satisfying $| J_1(x,y) \times J_2(x,y) | \neq 0$ must be applied [*Kwon O. et al, IEEE Trans. on BME 49: 160-167 (2002)*]. Vertical and horizontal current injection cases are applied and a combined sensitivity matrix is used.

For the animal experiments, a R3230 tumor induced rat was used. Four non-magnetic ECG electrodes were placed to left, right, top and bottom of the rat around the abdomen as shown in Figure 1(a). The locations of the electrodes were estimated from a regular spin echo image. Current carrying wires were placed parallel to z-direction and fixed to the frame.

Results

First, a standard spin echo image given in Figure 1(b) is acquired. The 2D FEM mesh generated with the boundary information extracted from this image (Figure 1(a)) contains 607 nodes and 1096 first order triangular elements. Electrode positions are also found from the spin echo image. For the MR-EIT experiment, 2 cycles of 10mA (rms) 200Hz current were injected into the rat and two phase images were acquired for two current injection cases using TR = 500ms, TE = 30ms, and NEX = 2. After calculating the sensitivity matrix for the generated mesh, inverse problem of MR-EIT was solved. Basis vectors corresponding to singular values less than 1/25 of the maximum singular value were truncated in matrix inversion and the conductivity image in Figure 1(c) was reconstructed.
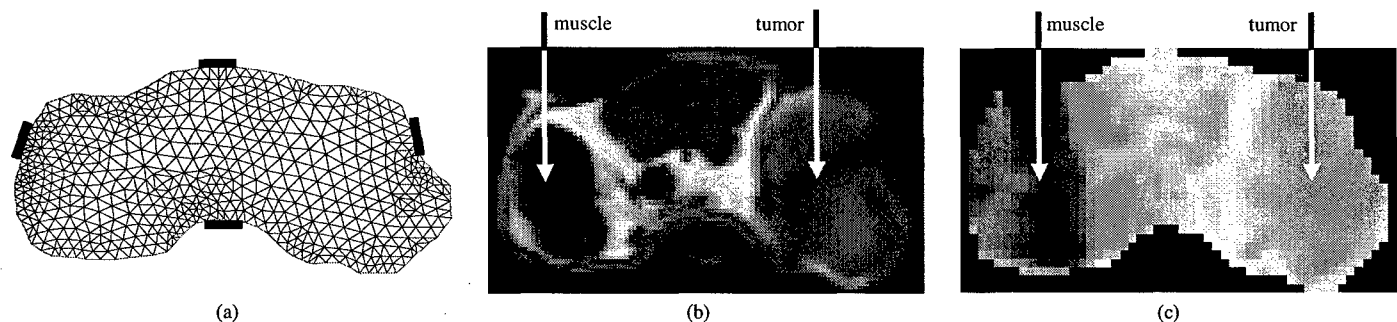

Figure 1 (a) FEM mesh and electrode positions (b) Spin echo image (c) Conductivity image

Discussion

In this preliminary study, we demonstrated that MREIT has the potential to be used as a diagnostic tool for detecting malignancies. This was a pilot study to assess its potential and limitations in-vivo. As seen in the figures above, the tumor region shows higher intensity, that corresponds to higher conductivity and the muscle region shows low intensity showing low conductivity. We expected higher conductivity in the tumor regions but volume of the lesion was large, thus a necrosis might have formed in the center, reducing the conductivity. It has previously been shown that impedance is much lower for lesions of smaller sizes. The high conductivity region next to the tumor could be an edema. We will conduct a longitudinal study on a large group of animals with lesions to observe impedance changes as the tumors grow. An advantage of the proposed method is that it does not require rotation of the animal inside the magnet to obtain orthogonal components of the magnetic field. In the reconstruction we have used a 2D finite element model (FEM), but we are currently working on a 3D FEM to further refine images. We are also working on placing MR observable markers to better localize electrode positions, which will also improve image quality and accuracy. We have also conducted phantom experiments to assess the limits and resolution of this method. It is submitted concurrently with this report.

A Comparison of MRI Based Electrical Impedance Imaging and Contrast Enhanced MRI of Tumors

L. Muftuler[1], M. Hamamura[1], O. Birgul[1], O. Nalcioglu[1]

[1]Functional Onco-Imaging Center, University of California, Irvine, CA, United States

Purpose

Malich et al has reported that the electrical impedance of malignancies could be 20-40 times lower than healthy tissues and benign formations [*Malich A. et al, Eur. Radiol. 10: 1555-1561 (2000)*]. Therefore, in-vivo impedance imaging of suspicious lesions could aid in improving the sensitivity and specificity of detecting malignant tumors. MRI based impedance imaging is a novel method, in which weak electrical currents are injected into the tissue and the resulting perturbations in magnetic field were measured using MRI. On the other hand, contrast enhanced imaging is a well-established method to detect malignant tissues. Since vascular growth is greatly enhanced in tumor structures, contrast agent uptake of tumor sites are increased with respect to normal tissues. In addition to that, interstitial compartment in tumors are larger compared to normal structures, so wash-out of contrast agent is also slower in tumors. Therefore, if two images are collected, one pre-contrast and the other post-contrast, the difference image will yield enhanced pixel intensity in the areas of tumor growth. In this study, our goal is to verify the potential of MR-EIT to detect tumors.

Methods

Sinusoidal current is injected into an object and the resulting magnetic fields are measured using a modified spin-echo sequence (Fig. 1) [*Mikac U. et al, MRI 19: 845 856 (2001)*]. The z-component of magnetic field (parallel to the main static field) generated by injected currents introduces a phase shift. By synchronizing successive π pulses to half cycles of the current, this phase shift accumulates and is given in the final image as $\varphi(\mathbf{r}) = 4\cdot\gamma\cdot N\cdot b(\mathbf{r}) / \omega$, where γ is the gyromagnetic ratio, N the number of cycles of injected current, $b(\mathbf{r})$ the amplitude of z-component current-generated magnetic field at point $\mathbf{r}$, and ω the angular frequency of the injected current. Hence, measurement of this phase shift allows for calculation of the (z-component) magnetic field distribution. To reconstruct conductivity image, a linear approximation $\Delta B(\mathbf{r}) = S(\mathbf{r},\mathbf{r}') \Delta\sigma(\mathbf{r}')$ is assumed, where $\Delta B(\mathbf{r})$ is the change in magnetic field at point $\mathbf{r}$ for a given current injection scheme resulting from a change $\Delta\sigma(\mathbf{r}')$ in the conductivity at point $\mathbf{r}'$. S is calculated using Finite Element Method (FEM). The matrix component S_{ij} is the change in magnetic field ∂B_i of element i with respect to a change in the

Fig. 1. Pulse sequence used in MR-EIT

conductivity $\partial\sigma_j$ of element j. An initial conductivity distribution σ_0 is assumed (e.g. uniform conductivity), the conductivity of a given element j is perturbed by $\Delta\sigma_j$ and the resulting ΔB is calculated. S is inverted to obtain $\Delta\sigma = \sigma_{final} - \sigma_{initial} = S^{-1} \Delta B = S^{-1} (B_{final} - B_{initial})$, where $\sigma_{initial}$ is the assumed initial (uniform) conductivity distribution, $B_{initial}$ the magnetic field distribution given $\sigma_{initial}$, σ_{final} the actual conductivity distribution, and B_{final} the MRI measured magnetic field distribution. Hence, the conductivity distribution of an object is $\sigma_{final} = S^{-1} (B_{final} - B_{initial}) + \sigma_{initial}$.

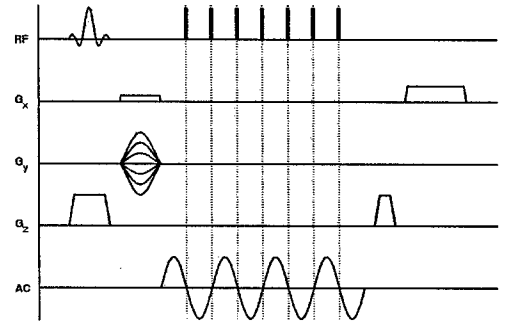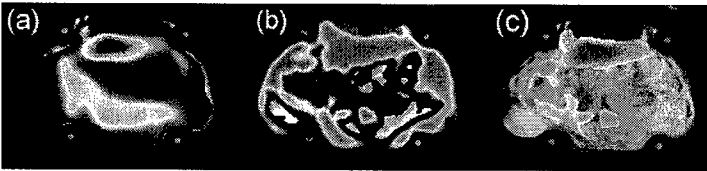Fig.2. (a) Conductivity distribution. Red: high conductivity, blue: low conductivity; (b) difference of pre and post Gd-DTPA images. Red: regions enhanced by Gd-DTPA; (c) Areas that have both high conductivity and also enhanced by contrast agent.

Results

An anatomical image was collected using FSE sequence prior to MR-EIT images. The data matrix was 256X256, FOV = 10cm, slice thickness = 6mm TR = 4s, TE = 20ms/100ms NEX = 4. MR-EIT images were collected using the previously outlined pulse sequence with TR=2s, TE=32ms, and NEX=8, 64X64 data matrix, FOV = 10cm, slice thickness = 6mm, with an AC current of 1mA peak, 200Hz, 4 cycles. Contrast enhanced images were collected using GE sequence with 64X64 data matrix, FOV = 10cm, 6mm slice thickness, TR = 150ms TE = 5ms and 45° flip angle. One pre-contrast image was acquired before Gd-DTPA injection and a post-contrast image was collected 3 minutes after injection. Relative conductivity distribution was computed as described above and overlaid on anatomical image (Fig. 2a). The resulting images clearly show the higher conductivity regions. Similarly, the contrast enhancement by Gd-DTPA is illustrated in Fig. 2b. Fig 2.c. shows regions that have high conductivity and also enhanced by Gd-DTPA. This image is generated by masking Gd-DTPA images with regions that have conductivity values in the upper one-third of the full range.

Discussion

In this preliminary study, we have shown that MRI based impedance imaging can be used to detect malignant tumors. It can be seen from these results that there is high correlation between conductivity images and contrast enhanced images. Although they do not completely overlap, this is expected because the two methods emphasize different properties of tumors. For example, edema will most likely show high conductivity but will not show signal enhancement with Gd-DTPA. To exclude edema regions from conductivity images, one can use T2 weighted sequences that highlights edema. In this preliminary experiment, we imaged an animal with a large tumor size, which was currently available. In large tumors, various compartments like edema, necrosis and viable tumor cells exist and their conductivity and contrast agent enhancement will be different. Currently we are working on a longitudinal study to observe changes in conductivity as well as Gd-DTPA based contrast enhancement in tumor structures as the tumor grows. Gd enhanced images will be used to verify our results in vivo. At the end of the study, tumors will be excised and undergo histologic analysis. Contrast enhanced and T2 weighted images together with MR-EIT maps will allow us to assess how conductivity correlates with different compartments of tumors. Electrode position and number could be another factor that may confound detection of some low conductivity structures close to surface. We will also investigate effects of electrode placement in our future experiments.

MRI Based Electrical Impedance Imaging of Tumors with Iterated Sensitivity Reconstruction Using Regularization

L. T. Muftuler[1], M. J. Hamamura[1], O. Birgul[1], O. Nalcioglu[1]

[1]Tu & Yuen Center for Functional Onco-Imaging, University of California, Irvine, CA, United States

Purpose

Several researchers have demonstrated that the electrical properties, specifically the impedance of malignant tissues is significantly different from those of normal and benign tissues [Malich *et al, Clin.Rad.*,56:278-283, 2001; Silva *et al. Med. Biol. Eng. and Comp.*, 38:26-30, 2000]. Therefore, *in vivo* impedance imaging of suspicious lesions could aid in improving the sensitivity and specificity of detecting malignant tumors. MRI based impedance imaging is a novel method, in which weak electrical currents are injected into the tissue and the resulting perturbations in magnetic field were measured using phase information in MR images. We have reported our preliminary studies with phantoms as well as some *in vivo* experiments. However, in those studies, reconstruction was done with the non-iterative sensitivity matrix approach, which assumed a linear relationship between the measured field perturbations and relative conductivity distribution. For large conductivity variations, this linearity assumption failed and the resulting images underestimated the conductivity variations. This resulted in poorer spatial specificity and sensitivity. We refined our reconstruction technique with an iterative approach to account for the nonlinearities. The goal is to verify potential of MR-EIT to aid in the diagnosis of tumors.

Methods

When a sinusoidal current is injected into an object, the z-component of the resulting magnetic fields induce additional phase information in MR images. A modified spin-echo sequence was used, where several π pulses were applied during the zero-crossings of the sinusoidal current (Fig.1) [Mikac *et al, MRI 19: 845 856 (2001)*]. This phase shift accumulates across these π pulses and is given in the final image as $\varphi(\mathbf{r}) = 4 \cdot \gamma \cdot N \cdot b_z(\mathbf{r}) / \omega$, where γ is the gyromagnetic ratio, N the number of cycles of injected current, $b_z(\mathbf{r})$ the amplitude of z-component of current-generated magnetic field at point $\mathbf{r}$, and ω the angular frequency of the injected current. Therefore, once the phase, $\varphi(\mathbf{r})$ is measured, $b_z(\mathbf{r})$ can be calculated. In the original approach, a linear approximation $\Delta B(\mathbf{r}) = S(\mathbf{r},\mathbf{r'}) \Delta\sigma(\mathbf{r'})$ was assumed to reconstruct conductivity image. Here $\Delta B(\mathbf{r})$ is the change in magnetic field at point $\mathbf{r}$ for a given current injection scheme resulting from a change $\Delta\sigma(\mathbf{r'})$ in the conductivity at point $\mathbf{r'}$. S is calculated using Finite Element Method (FEM). Recently, we have adopted an iterative reconstruction with Tikhonov regularization, which improved the accuracy as well as spatial specificity of the MREIT images. Details of this method and its assessment with phantom studies were presented in another manuscript that is being submitted concurrently. In

Fig. 1. Pulse sequence used in MR-EIT

summary, the matrix equation was modified with the addition of a *regularization parameter*, λ, and became $(S^T \Delta B = (S^T S + \lambda I) \Delta\sigma)$, where I is the identity matrix. This equation was solved for different values of λ using conjugate gradient method and the optimum value of λ was found. The conductivity distribution that is calculated after each iteration was assigned as the initial value for the next iteration and the iterations are repeated until the difference between the results of two consecutive iterations are below a predefined threshold. Current was injected from four electrodes placed across the animal's body and six different current distributions were generated by using different combinations of electrode pairs. This scheme also improved the uniformity and sensitivity of the MREIT images.

Results

Data were collected in a whole body 4T MRI system with a MRRS console. Two rats were imaged, which were bearing malignant tumors induced by the carcinogen ENU. Animals were anesthetized prior to imaging. All procedures were approved by the IACUC. Structural images were collected using SE sequence prior to MREIT images. The data matrix was 128X128, FOV = 10cm, slice thickness = 4mm, with 2mm gap. TR = 3s, TE = 50ms and NEX = 2 were used. MREIT images were collected using the previously outlined pulse sequence with TR=500ms, TE=30ms, and NEX=12, 64X64 data matrix, FOV = 10cm, slice thickness = 4mm with 2mm gap. 2 cycles of 100Hz current with 2mA rms was applied through different pairs of four electrodes. The resulting images clearly show the higher conductivity regions. Especially in animal-1, higher conductivity map of the tumor precisely overlaps with the one seen in the structural image. The mean conductivity in the tumor region was 2.8 times higher than the mean conductivity in the rest of the body for animal-1.
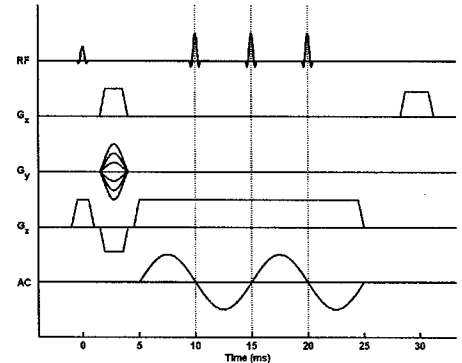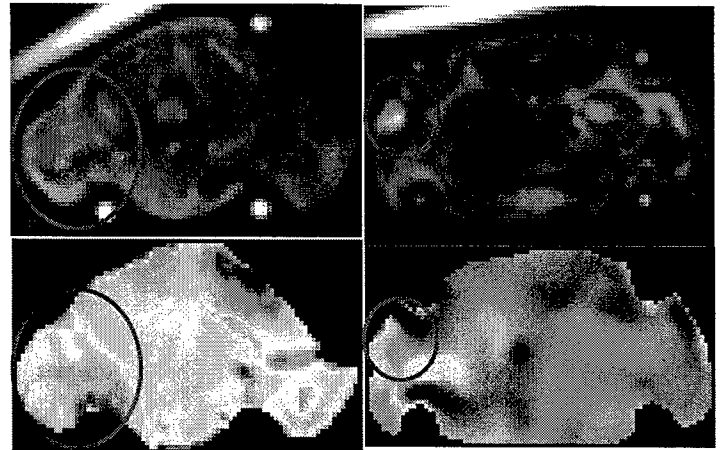

Fig.2. Structural (top) and MREIT (bottom) images of two animals. Left and right columns show the images of animal-1 and animal-2, respectively. Tumor areas are circled with red lines. Bright objects outside the animals were markers to identify exact location of electrodes.

Discussion

In this study, it has been demonstrated that MRI based impedance imaging has the potential to investigate malignant tumors *in vivo*. Improvements in current injection and utilization of iterative reconstruction with regularization significantly improved the accuracy and spatial specificity of MREIT. In our experiments it was also observed that precise localization of electrode placement was critical to define boundary conditions accurately, which in turn affected the quality of MREIT images. In the presented study, 2D FEM formulation was used. Currently 3D FEM is being developed to improve the accuracy of MREIT images further.

Acknowledgements:

Tracking of Sodium Diffusion in Agarose Using MR-EIT

M. J. Hamamura[1], L. T. Muftuler[1], O. Birgul[1], O. Nalcioglu[1]

[1]Tu & Yuen Center for Functional Onco-Imaging, University of California, Irvine, CA, United States

Purpose

It has been reported that the electrical impedance of malignancies is 20-40 times lower than healthy tissues and benign formations [*Malich A. et al, Eur. Radiol. 10: 1555-1561 (2000)*]. Therefore, *in vivo* impedance imaging of suspicious lesions could aid in the diagnosis of malignant tumors. In MR-EIT, electrical currents are injected into an object and the resulting magnetic field perturbations are measured using MRI. These measurements are then used to reconstruct the conductivity distribution within the object. Previous studies on MR-EIT have focused on reconstructing static conductivity distributions. However, the ability to detect changes in conductivity over time could provide additional diagnostic information, such as in monitoring tumor growth. In this study, we assess the ability of MR-EIT to detect these changes.

Methods

Sinusoidal current is injected into an object and the resulting magnetic fields are measured using a modified spin-echo sequence (Figure 1) [*Mikac U. et al, MRI 19: 845-856 (2001)*]. The component of current-generated magnetic field parallel to the main static field (z-component) introduces a phase shift. By synchronizing successive π pulses to half cycles of the current, this phase shift accumulates and is given in the final image as $\varphi(\mathbf{r}) = 4 \cdot \gamma \cdot N \cdot b(\mathbf{r}) / \omega$, where γ is the gyromagnetic ratio, N the number of cycles of injected current, $b(\mathbf{r})$ the amplitude of z-component current-generated magnetic field at point $\mathbf{r}$, and ω the angular frequency of the injected current. Hence, measurement of this phase shift allows for calculation of the (z-component) magnetic field distribution.

To reconstruct the conductivity distribution from the magnetic field distribution, a linear approximation $\Delta B(\mathbf{r}) = S(\mathbf{r},\mathbf{r'}) \Delta\sigma(\mathbf{r'})$ is assumed, where $\Delta B(\mathbf{r})$ is the change in magnetic field at point $\mathbf{r}$ for a given current injection scheme resulting from a change $\Delta\sigma(\mathbf{r'})$ in the conductivity at point $\mathbf{r'}$. The matrix component S_{ij} is the change in magnetic field ∂B_i of element i with respect to a change in the conductivity $\partial\sigma_j$ of element j. An initial conductivity distribution $\sigma_{initial}$ is assumed (e.g. uniform conductivity), the conductivity of a given element j perturbed by $\Delta\sigma_j$, the resulting ΔB calculated using the Finite Element Method (FEM), and the matrix components approximated as $S_{ij} = \Delta B_i / \Delta\sigma_j$. The linear approximation can be rewritten as $(\mathbf{B}_{final} - \mathbf{B}_{initial}) = S (\sigma_{final} - \sigma_{initial})$, where $\sigma_{initial}$ is the assumed initial (uniform) conductivity distribution, $\mathbf{B}_{initial}$ the FEM calculated magnetic field distribution given $\sigma_{initial}$, $\mathbf{B}_{final}$ the MRI measured magnetic field distribution, and σ_{final} the actual conductivity distribution. The equation is solved for σ_{final} using Tikhonov regularization. This σ_{final} then substituted back into the linear approximation as the new, updated $\sigma_{initial}$, and the process is iterated until the change in conductivity between successive iterations is below some predefined threshold. Details of this reconstruction method can be found in another abstract submitted concurrently.

The previously outlined method was used to measure the conductivity distribution of an agarose gel phantom. For the phantom, a hollow acrylic disk with an inner diameter of 7cm and thickness of 1cm was filled with 1% (g/100mL) agarose and 1% NaCl. Within this disk, a smaller circular region of 12mm diameter was filled with 1% agarose and 20% NaCl (Figure 2a). Over time, NaCl diffused from the region of higher concentration to the region of lower concentration. Conductivity is assumed proportional to NaCl concentration, hence the conductivity distribution changed as a result of this diffusion. The plane of the disk was placed perpendicular to the z-axis. Four recessed electrodes each 3mm wide were placed equidistant along the circular acrylic wall and used to inject currents into the interior region. Data was collected for two different current injection schemes (in pairs of electrodes directly opposite of each other) and used simultaneously in conductivity reconstruction.
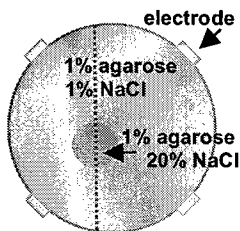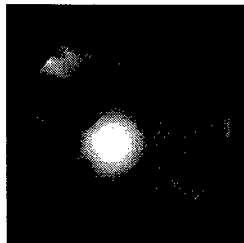

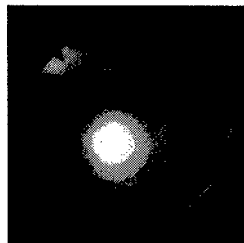*Figure 1. Pulse sequence used in MR-EIT*

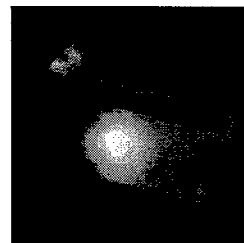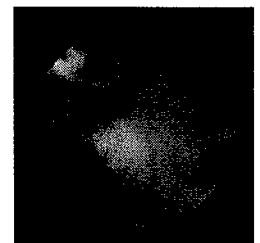*Figure 2a* *Figure 2b* *Figure 2c* *Figure 2d* *Figure 2e*

Figure 2. (a) Schematic of the phantom; (b) Conductivity after 20 minutes; (c) 1 hour; (d) 6 hours; (e) 24 hours

Results

2 cycles of 10mA (rms) 100Hz current were injected into the phantom using the previously outlined pulse sequence with the parameters TR=500ms, TE=30ms, and NEX = 4. Scans were taken 20 minutes, 1 hour, 6 hours, and 24 hours after the creation of the phantom. The z-component current-generated magnetic field distributions were calculated from the resulting data and the conductivity distributions computed (Figures 2d-e). The resulting images clearly show a change in the conductivity distribution consistent with the diffusion of NaCl from the higher concentration region to the lower concentration region. Over time, the higher conductivity region broadens, and the border between the initial regions becomes less distinct (Figure 3).

Discussion

In this study, we have shown that MR-EIT can be used to monitor changes in conductivity over time. While we assume that conductivity is directly proportional to NaCl concentration for this phantom, future studies will verify this by correlating this method with Sodium MRI. We also plan to monitor malignancies in live animals by performing MR-EIT measurements over the span of several weeks.

Acknowledgement
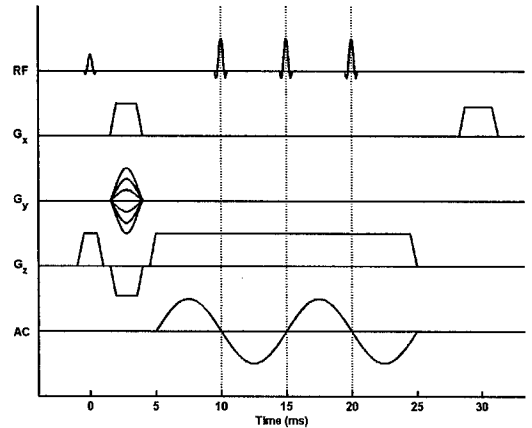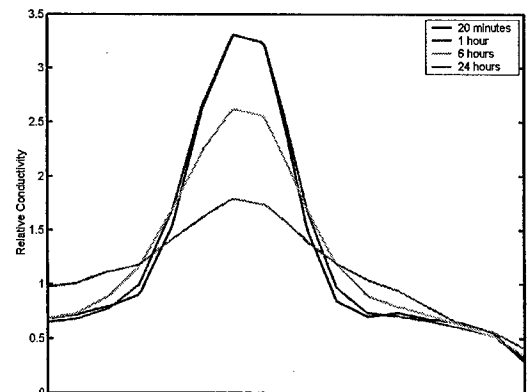
Figure 3. Profile taken across the dotted red line of Figure 2a